

THIS REPORT HAS BEEN DELIMITED
AND CLEARED FOR PUBLIC RELEASE
UNDER DOD DIRECTIVE 5200.20 AND
NO RESTRICTIONS ARE IMPOSED UPON
ITS USE AND DISCLOSURE.

DISTRIBUTION STATEMENT A

APPROVED FOR PUBLIC RELEASE,
DISTRIBUTION UNLIMITED.

Department of the Navy
Office of Naval Research Contract Nonr. 24475
and
Bureau of Ordnance Contract NOrd 9612

AD No. 36510
ASTIA FILE COPY

INCIPIENT CAVITATION AND BOUNDARY LAYER INTERACTION
ON A STREAMLINED BODY

E. R. Parkin and R. W. Kermeen

Hydrodynamics Laboratory
California Institute of Technology
Pasadena, California

Report No. E-35.2
December, 1953

Approved by:
M. S. Plesset

Contents

	<u>Page</u>
Abstract	1
Introduction	1
The Flow over the Model under Noncavitating Conditions	2
Preliminary Photographic Studies of Incipient Cavitation	4
High-Speed Motion Picture Study of Incipient Cavitation	10
The Role of Air Diffusion in Cavitation Inception	19
The Need for Further Pressure Measurements	22
The Shortcomings of Conventional Pressure Measurements	22
Membrane Method for Measuring Pressure	24
Tension Measurements at Incipient Cavitation	25
Conclusions	30
Appendix	33
A. Experimental Setup and Procedure	33
B. A Method for Securing Rubber Membranes to the Model	35
C. Proofing the Pressure Measuring Apparatus	36
References	43

Abstract

An experimental investigation of the effect of the boundary layer on cavitation inception for a smooth streamlined body of revolution is described. The influence of air diffusion upon the observed results is also discussed. In addition, this study has shown that tensions exist in the flow of ordinary water at incipient cavitation.

Introduction

The present report summarizes the results of our recent investigations on the effect of the boundary layer upon cavitation inception on a smooth streamlined body. The need for a detailed study of the inception mechanism was emphasized by the lack of agreement between our experimental observations for incipient cavitation scale effect^{1, 2} and a simplified theoretical analysis.³

One of the major simplifying assumptions of the theory was the hypothesis that the bubble nuclei moved over the body with the velocity of the water outside the boundary layer. From the systematic deviations between the calculated and experimental values of the incipient cavitation number, it appeared that this neglect of the boundary layer was not justified.

Observations of very small cavitation bubbles on a body upstream from the ordinarily observed band of incipient cavitation were first made during scale effect experiments in the High Speed Water Tunnel, and the first photographs of these bubbles were reported in Ref. 1. These observations provided the first direct evidence that the neglect of the boundary layer may account for a large part of the disagreement between theory and experiment.

The purpose of the present study is to investigate the mechanics of cavitation inception and the effect of the boundary layer in the hope that a complete theoretical explanation for the experimental observations might be developed. This report gives the first results of the general program and it indicates some of the questions which must be answered before the work may be considered complete.

The Flow over the Model under Noncavitating Conditions

A study of the mechanics of cavitation inception and the related boundary layer effects requires a knowledge of the magnitude and duration of the pressure forces acting on the cavitation bubbles as well as the properties of the boundary layer on the body. For the incipient state it seems likely that the pressures and the boundary layer thickness on the body are approximated by these quantities in noncavitating flow because the extent of cavitation on the body is very small. In addition to providing a basis of comparison for later measurements of cavitation, these experiments indicated the influence of the unusual position of the model in the working section on the cavitation experiments. In order to obtain better conditions for visual and photographic observation, the model was mounted near the working section window. The first experiments were made to determine the pressure distribution over the model in this position. The setup used in these tests is described in the Appendix, Section A.

The pressure distribution data were taken along meridional planes in five degree increments by rotating the model nose about its longitudinal axis (cf. Fig. 25). The pressure readings were reduced to pressure coefficient form,

$$C_p = \frac{p - p_0}{1/2 \rho V_0^2} ,$$

where p is the pressure at a point on the body, p_0 is the free stream static pressure, ρ is the water density, and V_0 is the free stream velocity. All C_p data were plotted against the meridional arc length S along the model for each value of θ as in Fig. 1. The minimum pressure coefficients from these graphs were plotted against θ in a polar diagram. Within the accuracy of the data, no asymmetry of minimum pressure with θ could be discerned, although the minimum pressure coefficient was -0.80 with the model near the wall compared with -0.74 for the model situated in the center of the working section. When a polar plot of C_p versus θ is constructed for a fixed distance from the model nose, in Fig. 2, a slight asymmetry is evident. This asymmetry results from a shift in the position of the point of minimum pressure with θ . However the greatest relative shift in the minimum pressure point appeared to be within 3% of the model diameter for all values of θ .

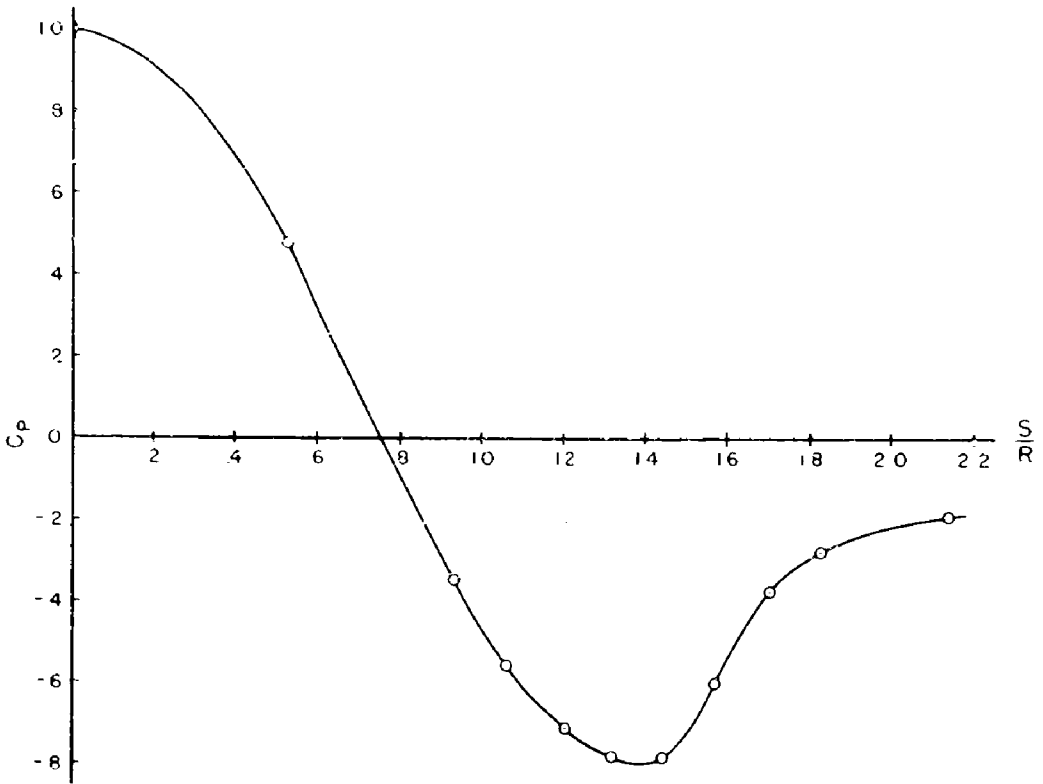


Fig. 1 - Pressure distribution in plane of pressure taps for $\theta = 90^\circ$.

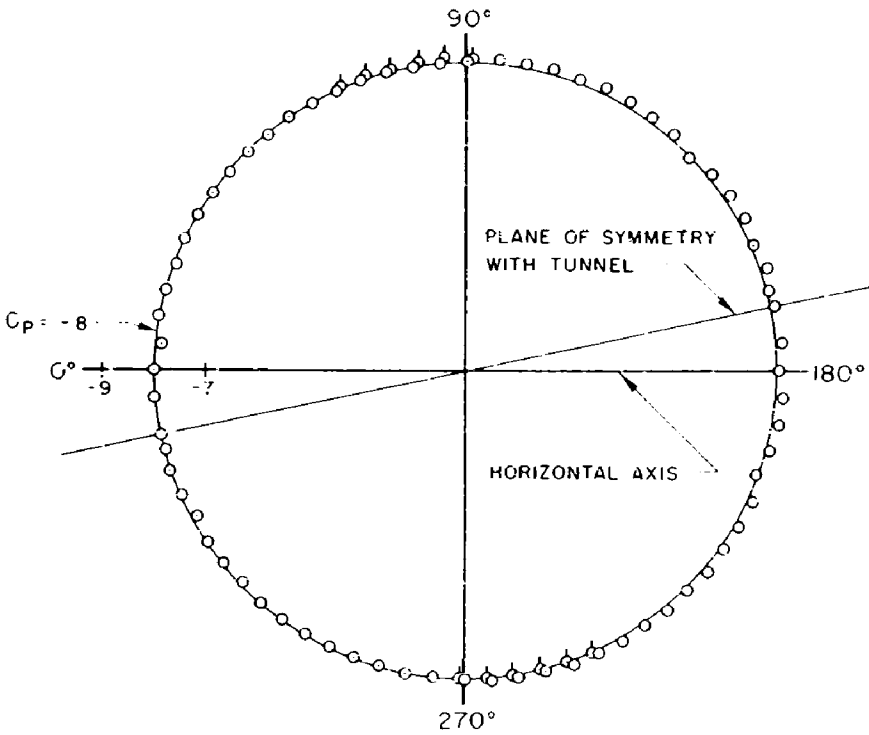


Fig. 2 - Pressure distribution vs polar angle θ at a constant $S/R = 1.378$ (at cross section A-A of Fig. 22)

From Eisenberg's results⁴ on the flow about an ellipsoid near a plane wall one would expect appreciable asymmetry in the azimuthal distribution of the minimum pressure. However these experiments differed from those of Eisenberg in that the boundary layer thickness was about one-fourth of the model diameter. In Eisenberg's experiment the boundary layer was small compared to the diameter of the ellipsoid because he used a short flat plate to simulate the wall, while in the present experiments the tunnel wall allowed considerable distance for boundary layer growth. Even though the hemisphere was placed far enough from the wall to be well out of the tunnel wall boundary layer, we believe that the nearly axially symmetrical pressure distribution resulted from this region of slow-moving fluid near the model.

In view of the nearly axially symmetric pressure distribution on the body, the boundary layer thickness was calculated as though the model were in axially symmetric flow. The method of C. B. Millikan⁵ was used for these calculations because it is believed that this method gives enough accuracy for the present requirements. Although the flow over the model was probably not truly axially symmetric, a more refined method of calculation did not seem warranted. The calculations were based on the pressure distribution of Fig. 1 for $\theta = 90^\circ$. The calculated boundary layer thickness was 0.0047 in. at the minimum pressure point, $S/R = 1.4$, and grew to 0.0075 in. at the nose-cylinder tangent point, $S/R = \pi/2$.

The zone of laminar-turbulent boundary layer transition for noncavitating flow was also determined. Estimates for the approximate upstream limits to be expected were calculated from the small oscillation theory for laminar boundary layer stability. The expected downstream limits were calculated from the usual empirical critical boundary layer Reynolds number criterion. The actual position of the transition zone was experimentally determined (see Appendix, Section A) to lie between the two calculated values. These observations showed that transition occurred in the vicinity of the point where the hemisphere joins the cylindrical body ($S/R = 1.571$).

Preliminary Photographic Studies of Incipient Cavitation

After determining the characteristics of the noncavitating flow over the model, the next phase of the investigation was to observe the very small

bubbles which had appeared to be in the boundary layer on the body. These observations of the cavitation bubbles at inception could then be related to the known properties of the noncavitating flow. This part of the program required a detailed study of cavitation bubble histories from the first onset of cavitation to the development of clear cavities attached to the model nose. Figure 3 shows the two stages of cavitation on a hemispherical model, intermittent bubbles on the left, and at a lower cavitation number, clear attached cavities on the right.

In order to simplify the photographic problems associated with recording the processes of incipient cavitation in the boundary layer, the first phases of the present work were restricted to still photographs at 5 and 8 times magnification. This technique provided greater flexibility and allowed inspection of results within a very short time after an exposure. All still photographs were taken with an Eastman 4 x 5 view camera, which was equipped with an f/4.5 Micro Tessar lens of 72 mm focal length. In order to obtain the required magnification, the lens-to-plate distance was extended by mounting the lens on an aluminum tube which was threaded to fit the front of the camera, Fig. 4. Exposures were made with Edgerton type flash lamps.

The majority of the still photographs were taken with back lighting so that the model profile appeared in silhouette. This arrangement allowed us to relate the cavitation to the surface of the model and the boundary layer thickness. Since a black anodized aluminum model was used for all photographic studies, we were also able to take some double exposures which were not profile views. These pictures were used to estimate the bubble transport velocities from knowledge of the time interval between flashes. All photographs were taken with the free stream velocity, V_o , set at 40 fps. The degree of cavitation on the body was altered by changing the free stream static pressure, p_o .

Figures 5a and 5b show a typical profile photograph taken at an image to object magnification of 8 to 1 and are further enlarged in these illustrations. The cavitation number

$$K = \frac{p_o - p_v}{1/2 \rho V_o^2}$$

was 0.735 for this picture. In the expression for K , p_v is the water vapor pressure and ρ is the density of the water. The boundary layer quantities

which are superposed on this figure were calculated from the pressure distribution in noncavitating flow as described in the previous section. The region marked "laminar-turbulent transition zone" shows the extreme positions of the transition point as determined from the dye studies. The furthest downstream point ($S = 1.57''$) was then used for the initial point in approximate calculations for the turbulent boundary layer displacement thickness. Following the standard procedure, we specified that the momentum thickness should be continuous at the transition point. This causes a discontinuity in the displacement thickness at the transition point. The average displacement thickness was about 0.0017 in. in the turbulent region. In the interest of simplicity, none of the turbulent boundary layer quantities were included in Fig. 5.

The important feature shown by Fig. 5 is the small bubbles which are growing in the boundary layer upstream of the fuzzy macroscopic cavitation. Under ordinary conditions of observation only the foamy patch is visible to the unaided eye, and when such regions of macroscopic cavitation first appear one uses the term "incipient cavitation". As can be seen from the photograph, the largest of the small bubbles is only about 0.002 in. in diameter. Further, these small bubbles make their first appearance downstream of the minimum pressure point. In fact, they are first visible at points on the body where the pressure is greater than the vapor pressure ($C_p < -K = -0.735$). This would indicate that the growth of the small bubbles could start upstream from the region where they were first seen and that their growth in the downstream region might occur because of the inertia of the water outside of the expanding bubbles. The motion pictures which followed the still shots could not provide us with bubble growth histories. The image magnification was not great enough and in all cases the photographic resolution was limited by the curved lucite water tunnel window. Accordingly, the investigation of such bubble growth histories depends upon improved instrumentation for photographic observation. On the other hand, the observed bubble growths could result from air diffusion into the bubbles from the surrounding super-saturated water even if no inertial effects are operative. We will return to this question after we have discussed additional observations.

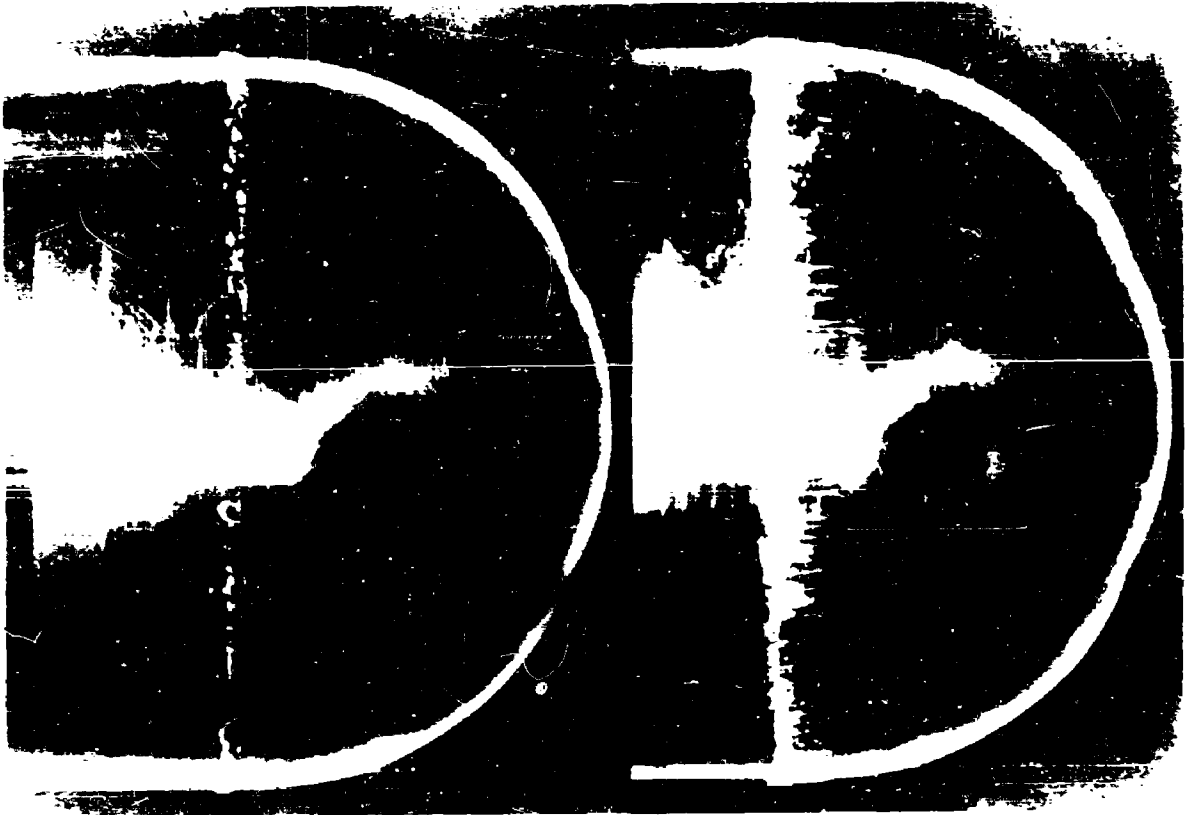


Fig. 3 - Cavitation on hemispherical head model. Intermittent bubbles left, and attached cavities at lower cavitation number, right.

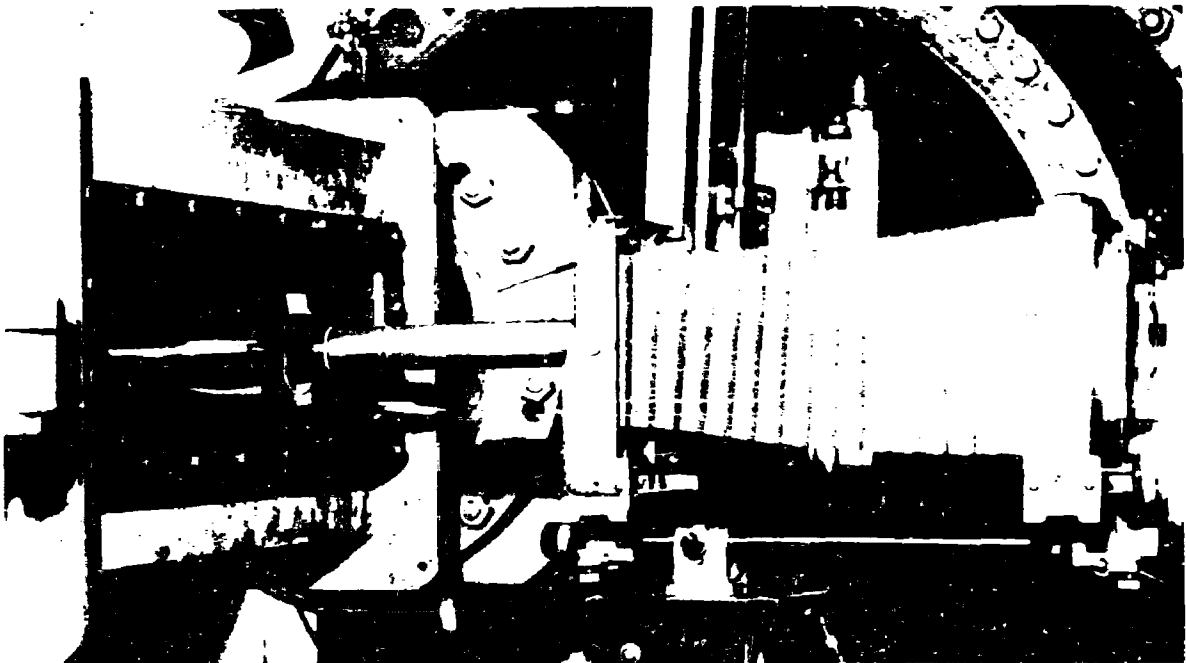


Fig. 4 - Camera setup for still photographs of cavitation. Note the lens extension which provides an 8x magnified image on photographic film. 72 mm Micro Tessar lens used.

In the next profile shot, Fig. 6, K has been lowered to a value (0.698) which allows the foamy patch to become a clear cavity. The leading edge of this cavity is attached to the body as shown. It is important to note that the presence of the clear cavity has entirely suppressed the small bubble growth. Evidently such attached, clear cavities are sustained by evaporation from the cavity wall and also by the diffusion of air into the cavity from the nearby liquid, as is the case for full cavity flows.

The two illustrations cited above typify the conditions encountered in all of the still pictures. In general, after cavitation was initiated, the number of small bubbles upstream of the macroscopic cavitation increased with decreasing cavitation number K until the clear cavity was well established. At this point small bubble growth was suppressed. Pressure fluctuations in the water tunnel working section tended to mask these effects but we believe that we have correctly described the essentials of the process. A change in dissolved air content from 7.6 parts per million to 16.3 parts per million made no detectable difference in these events.

It was noticed that the position on the body of the leading edge of the macroscopic cavitation changed with the cavitation number. Figure 7 shows the positions of the leading edge of the macroscopic cavitation zone plotted against the cavitation number. The figure shows that the large cavity moves forward on the body as K is decreased within the observed range. The scatter of the data was caused by pressure fluctuations in the flow. A two-fold change in the dissolved air content made no significant difference in the findings.

Figure 8 shows one of the double flash photographs at 8 to 1 magnification ratio. This was one of the several pictures which were measured to determine the bubble transport velocities. The cavitation number for this particular photograph was 0.710. The free stream velocity V_0 was 40 fps. The time interval between the two flashes was 0.53 milliseconds. We found that the bubbles appeared to have velocities over the model surface which ranged between 0.4 and 4.0 fps. Further, it seemed that the velocity depended on the bubble size and to a slight degree on its position on the body. The information obtained from the double exposures can only give crude estimates of the bubble transport velocities. Evidently these velocities are significantly less than the velocity of the liquid in the free stream and the small bubbles

remain in the boundary layer and are transported into the region of macroscopic cavitation.

High-Speed Motion Picture Study of Incipient Cavitation

The various factors which have been discussed in the previous section complete the results which can be obtained from the still photographs. We have seen that the small bubbles which definitely grow in the boundary layer are followed by a downstream region of macroscopic cavitation. It is when this macroscopic cavitation first appears on the body that we speak of incipient conditions. We have also seen how the character of the macroscopic cavitation changes as the cavitation number is lowered until no small bubbles grow in the boundary layer. Although the still photographs indicated that the foamy macroscopic cavitation is probably related to the small bubbles in the boundary layer, they could not supply definite proof. Further, no details of the small bubble transport motions and no accurate estimate for the transport velocities could be obtained. Therefore, high-speed motion pictures were taken under the same conditions of cavitation on the same model. The same Micro Tessar lens was used on the General Radio high-speed camera as was used for the still shots. The silhouette pictures were taken at image-to-object magnification ratios of 5 to 1 and 8 to 1. The repetition rate for all motion pictures was 6000 frames per second. The position of the camera with respect to the working section is shown in Fig. 9.

The magnified motion pictures provided us with more details of the events which occur during incipient cavitation. The results of the first measurements made from the films are shown in Fig. 10. This figure shows the bubble position on the model surface at each instant of time from that time t_0 at which a given bubble was first visible. It will be seen that the bubble transport history is characterized by two phases. During the first phase the bubble grows at a fixed point on the body. The second phase starts after the bubble has become sufficiently large and is lifted up slightly from the body. Then it is transported downstream and distorted into an irregular patch which feeds the macroscopic cavitation. The start of this second phase of the bubble motion is indicated by the sharp bend in each of the curves of Fig. 10. The curves end where the bubble has become distorted and has merged

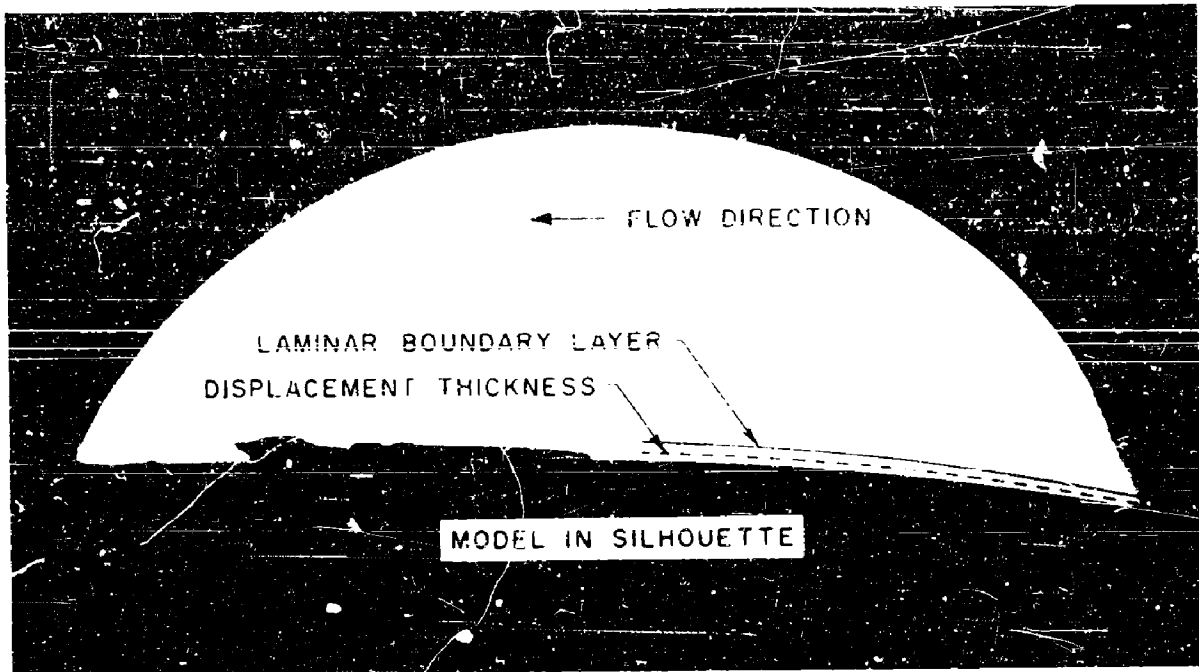


Fig. 6 - Photograph of clear attached cavity with boundary layer dimensions superposed.

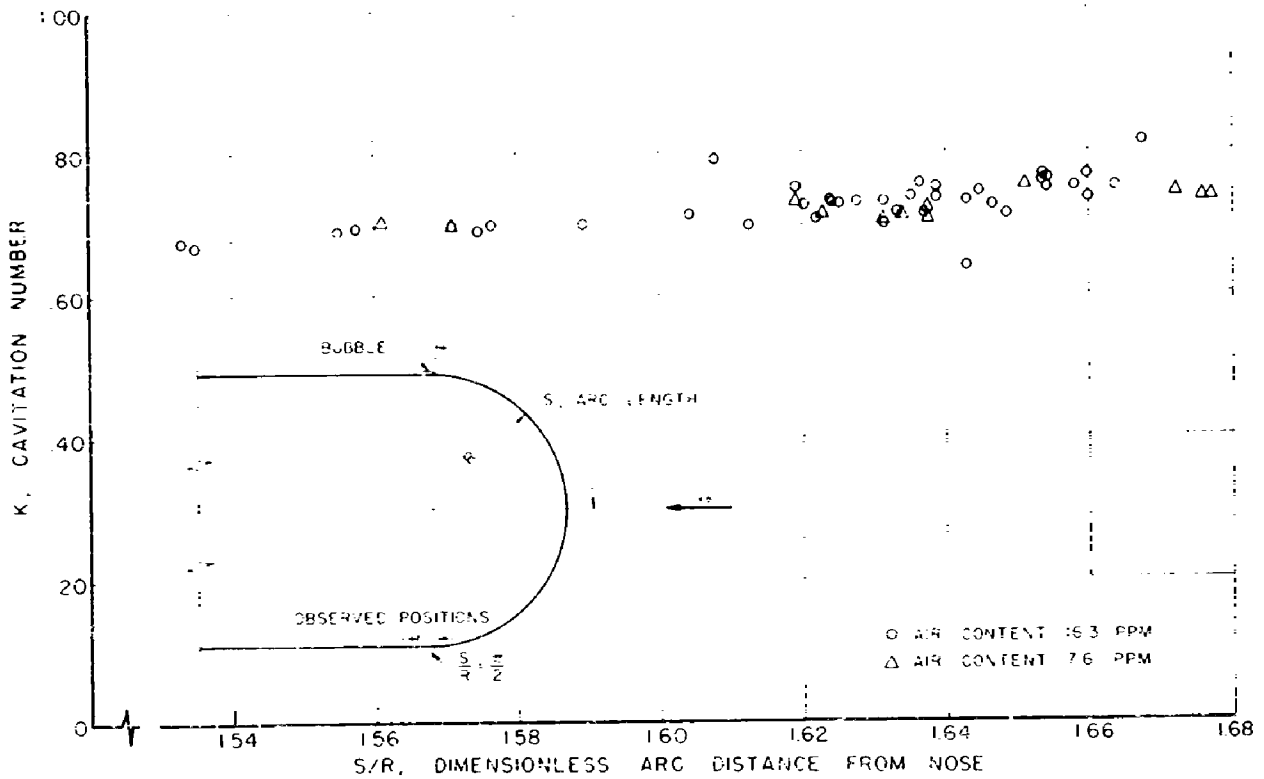


Fig. 7 - Position of the leading edge of the macroscopic cavitation as a function of cavitation number.

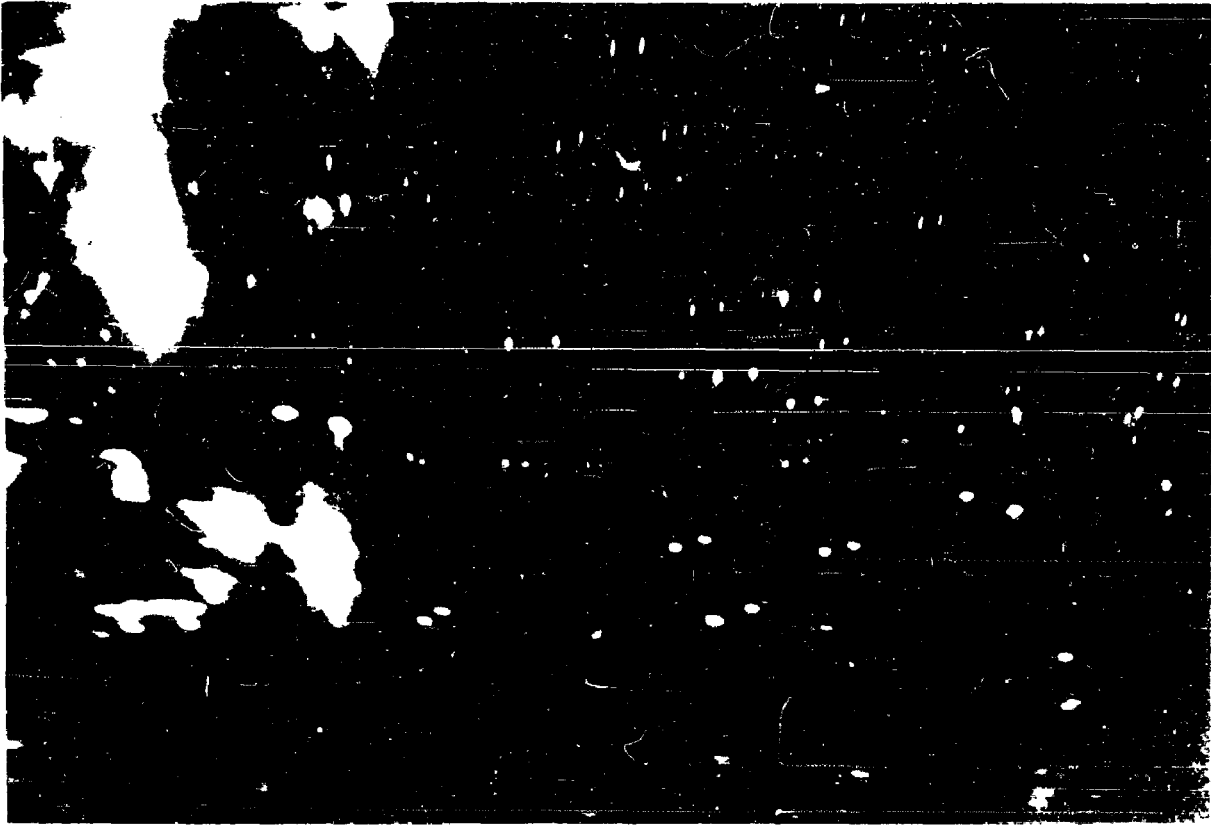


Fig. 8 - Double flash exposure of cavitation on black hemispherical nose. Time between flashes 1.2 millisecc.
 $K = .710$

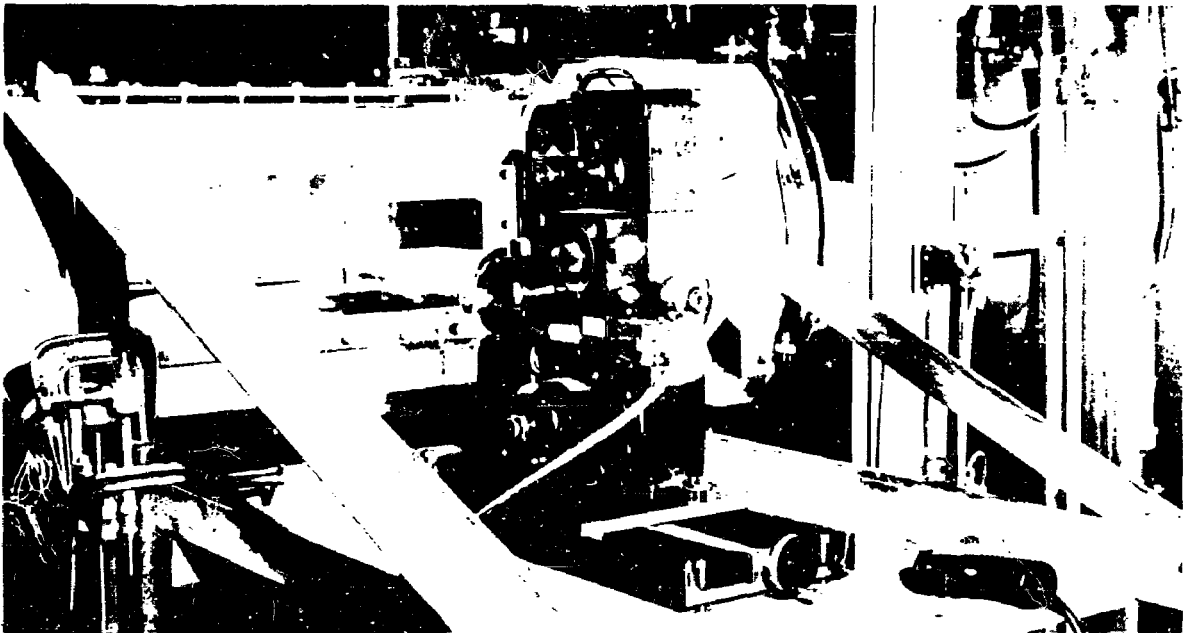


Fig. 9 - High-speed camera setup with lens extension and 72 mm Micro Tessar lens.

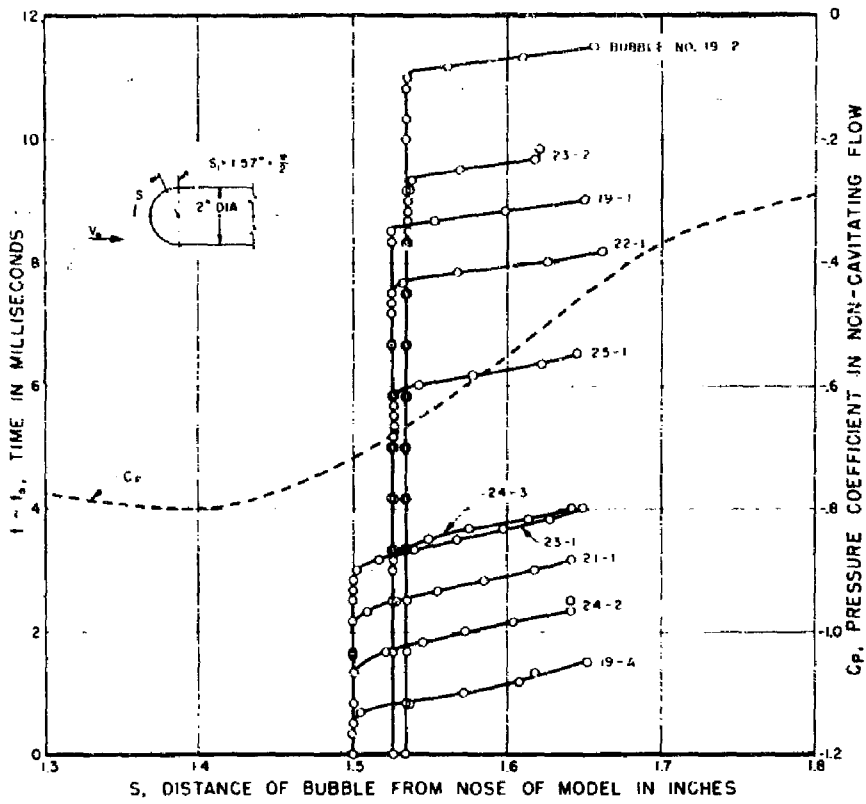


Fig. 10 - Position vs time curve for microscopic cavitation bubbles.

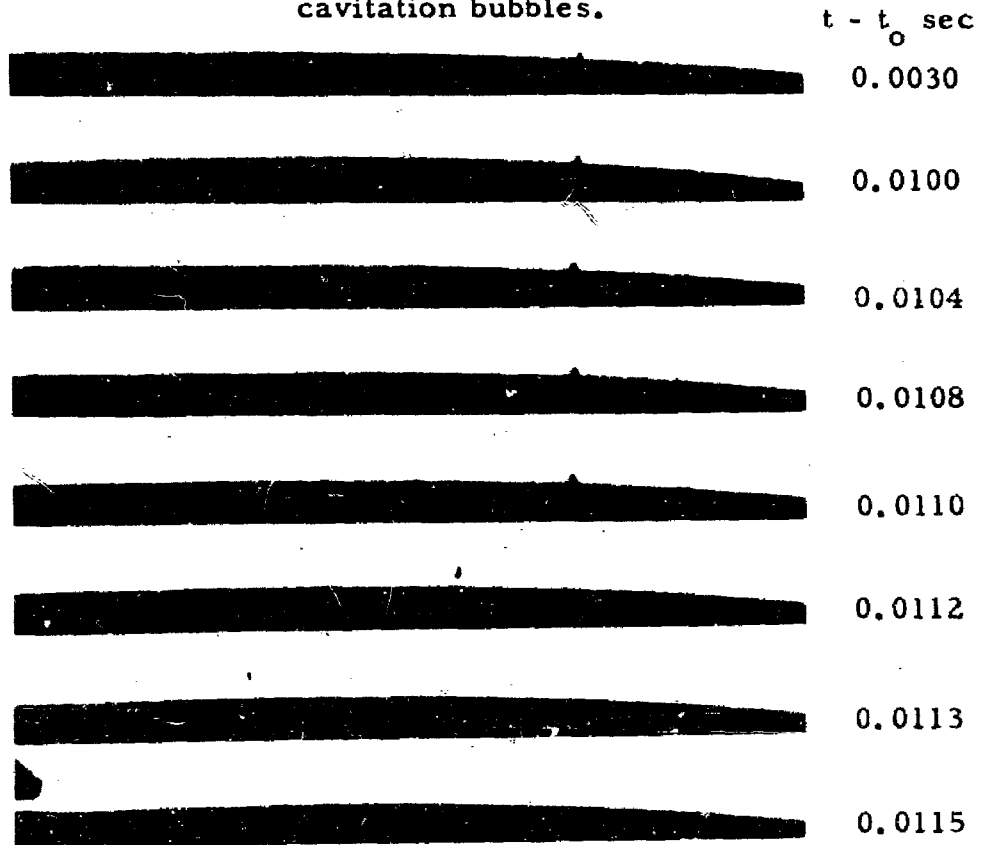


Fig. 11 - Microscopic cavitation bubble motion in the boundary layer. Bubble is No. 19-2 in Fig. 10.

into the irregular-shaped macroscopic cavitation. Figure 11 shows portions of the high-speed picture sequence of the microscopic bubble labeled 19-2 in Fig. 10. The first frame shows the position of the bubble at time $t = 3$ milliseconds after it first became visible. The second frame shows the bubble at $t = 10$ milliseconds. Succeeding frames show the second phase where the bubble is transported downstream and is distorted into a patch of macroscopic cavitation. These last frames correspond to the points of the curve in Fig. 10. The average transport velocity of the bubbles in Fig. 10 was 21 fps. One of these bubbles had the low velocity of 13 fps while two others had the high velocity of 26 fps. It is clear that the bubbles are well inside the boundary layer even during the transport phase since the free stream velocity ahead of the model was 40 fps. The fact that the small bubbles grow for a time at a fixed position on the body can account for the low, widely varying velocities estimated from the still photographs.

We cannot conclude that these small bubbles will be fixed with respect to all bodies during this growth phase. Other bodies will have different pressure gradients and somewhat different boundary layer properties from the particular shape studied here. However, microscopic cavitation has been observed on other bodies such as ogives and hydrofoils, although the effect of the boundary layer on incipient cavitation has not been investigated for these other shapes.

Figure 10 shows the histories of bubbles which have grown at three points on the model surface. It is noteworthy that, in general, the time interval required for the growth phase varied with the point on the body. Because the extent of the cavitation on the body is very small, the pressure distribution for noncavitating flow is probably little changed under these conditions of incipient cavitation. If this assumption is correct then the graph shows that the growth time decreases with decreasing pressure on the body. The variation in the growth time may also be correlated with cavitation number for each position on the body. Except for those bubbles which first appeared at $S = 1.5$ in., a definite correlation between the growth time $t_1 - t_0$ and the cavitation number was found. In the interest of clarity, only four of five bubbles which were first visible at $S = 1.5$ are shown on Fig. 10. Three of the five bubbles conformed to the expected correlation. The two effects which we have just discussed are simply manifestations of the obvious

fact that if the amount of growth is fixed, the time for this growth will vary with the pressure in the surrounding liquid. We will now turn to the reasons for supposing that the observed bubble growth was fixed.

One aspect of this question is the maximum size attained by the small bubbles before they are transported downstream. Also any relation between this maximum size and the characteristics of the boundary layer velocity profile would be of interest. Accordingly, measurements of bubble sizes just before breakaway from the body were made from the motion picture films. The results of these measurements are shown compared with the calculated displacement and momentum thicknesses for the given flow in Fig. 12. It can be seen that the bubbles grow to a size roughly equal to the displacement thickness. Probably a large part of the scatter in the measurements is due to the astigmatism in the bubble images produced by the plano-concave tunnel windows. Before definite conclusions can be made regarding this point, tests will have to be made on models with varying boundary layer thicknesses and under more favorable optical conditions.

This result shows that the bubbles of Fig. 10 all attained about the same diameter of 0.002 in. before they were transported downstream. In addition, the time intervals $t - t_0$ of Fig. 10 were measured from the time at which the bubbles were first visible. Since the lighting, lens setting and exposure were fixed during these experiments, it would appear that the smallest bubble size which could be recorded on the film was also fixed. Of course, the "initial" size of these small bubbles could not be measured because these first images bear no known relation to actual bubble size. However, we can conclude that each time interval $t_1 - t_0$ corresponded to a nearly fixed but unknown amount of bubble growth; where t_1 is that time which corresponds to the start of the downstream bubble motion.

Another aspect of the flow at cavitation inception is illustrated by Fig. 12. It shows that the microscopic bubbles grow in both laminar and turbulent regions of the boundary layer. The positions on the body where the bubbles have been observed and the relative position of the transition zone indicate that for these experiments, the mechanics of inception are not effected by transition in the boundary layer. Of course, the present experiments were not designed to examine this question, and additional experimental work is required to provide a complete answer.

Figure 13 shows the correlation that is obtained between the time interval $t_1 - t_0$ of Fig. 10 and the absolute pressure in the liquid on the body. The absolute pressures were calculated from the known pressure distribution for noncavitating flow at the given free stream velocity and static pressures. Aside from the two exceptional bubbles which showed no correlation with the cavitation number in Fig. 10, the pressure-time correlation in Fig. 13 is clear. This figure also shows that the bubbles are growing in regions where the pressure is greater than the vapor pressure of water. The reason for this behavior is discussed in the next section of this report.

In addition to the data on microscopic cavitation bubble histories, the high-speed motion pictures gave information on the other phases of cavitation. These high-speed photographs gave further evidence that microscopic bubble growth was suppressed at the onset of clear attached cavities and verified the results in Fig. 6 which shows the position of the leading edge of the cavity as a function of cavitation number.

So far only the primary interactions of the boundary layer and incipient cavitation have been considered. Now certain secondary bubble motions which appear to be caused by static pressure fluctuations in the tunnel working section will be discussed. At cavitation numbers slightly higher than that which produced a clear macroscopic cavity, certain of the microscopic bubbles were seen to move upstream in the boundary layer as shown in the motion picture sequence, Fig. 14. Then the forward motions of the bubbles would stop and they were lifted up and transported downstream over the top of the macroscopic cavity. A careful examination of the motion picture films showed that these bubbles were originally part of the macroscopic cavitation. When pressure fluctuations caused the leading edge of the macroscopic patch to move back and forth on the body, occasionally small portions of the leading edge would become detached and the sequence of events noted above was started. Evidently the upstream motion of these bubbles was a result of the lower pressure region upstream of the macroscopic region which we have found to exist at these cavitation numbers. In fact, noncavitating flow with a 40 ft/sec free stream velocity gives rise to an adverse pressure gradient in this area of the model which is forty times the hydrostatic gradient for still water, so these upstream motions are not surprising. The whole progress of a typical bubble in secondary motion is plotted in Fig. 15. The time position curve of Fig. 15 is for the bubble shown in Fig. 14. The initial time was

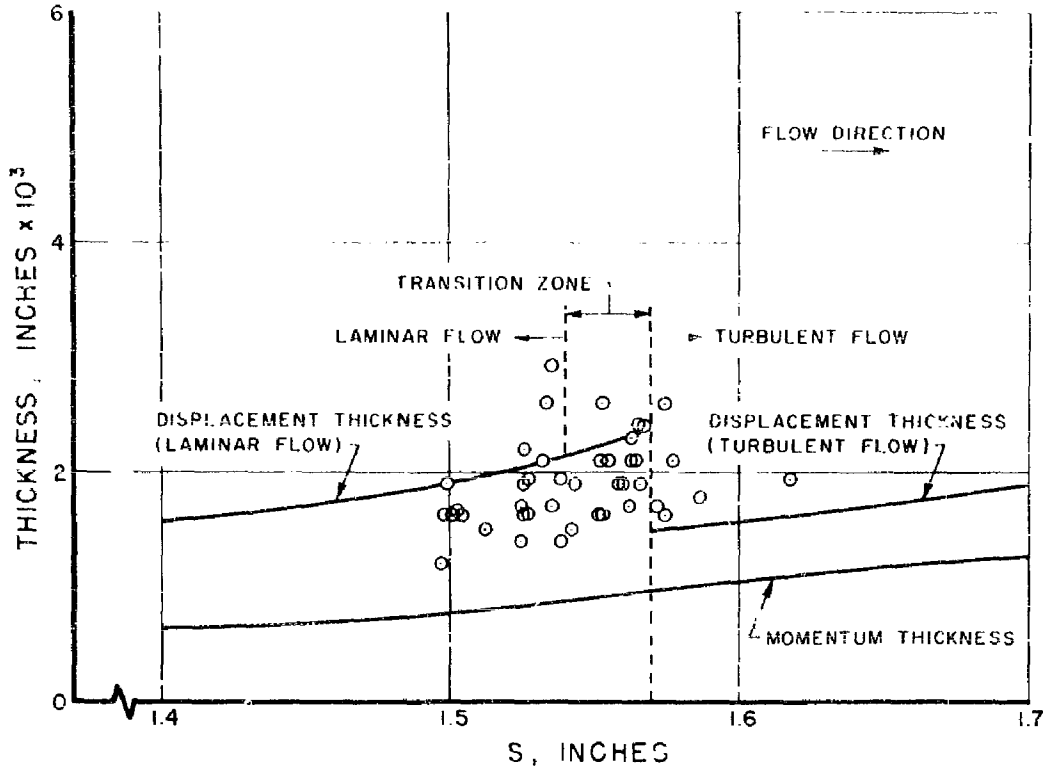


Fig. 12 - Maximum diameters attained by microscopic cavitation bubbles before moving downstream.

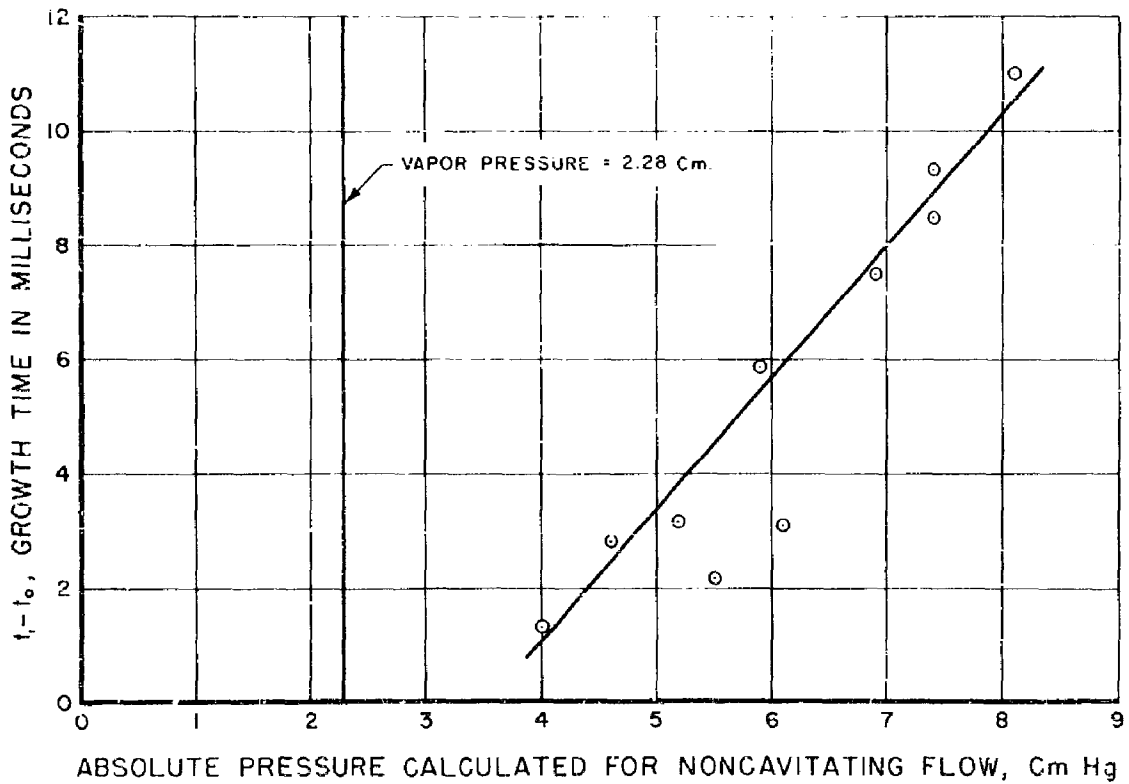


Fig. 13 - Growth time for microscopic cavitation bubbles as a function of absolute pressure.

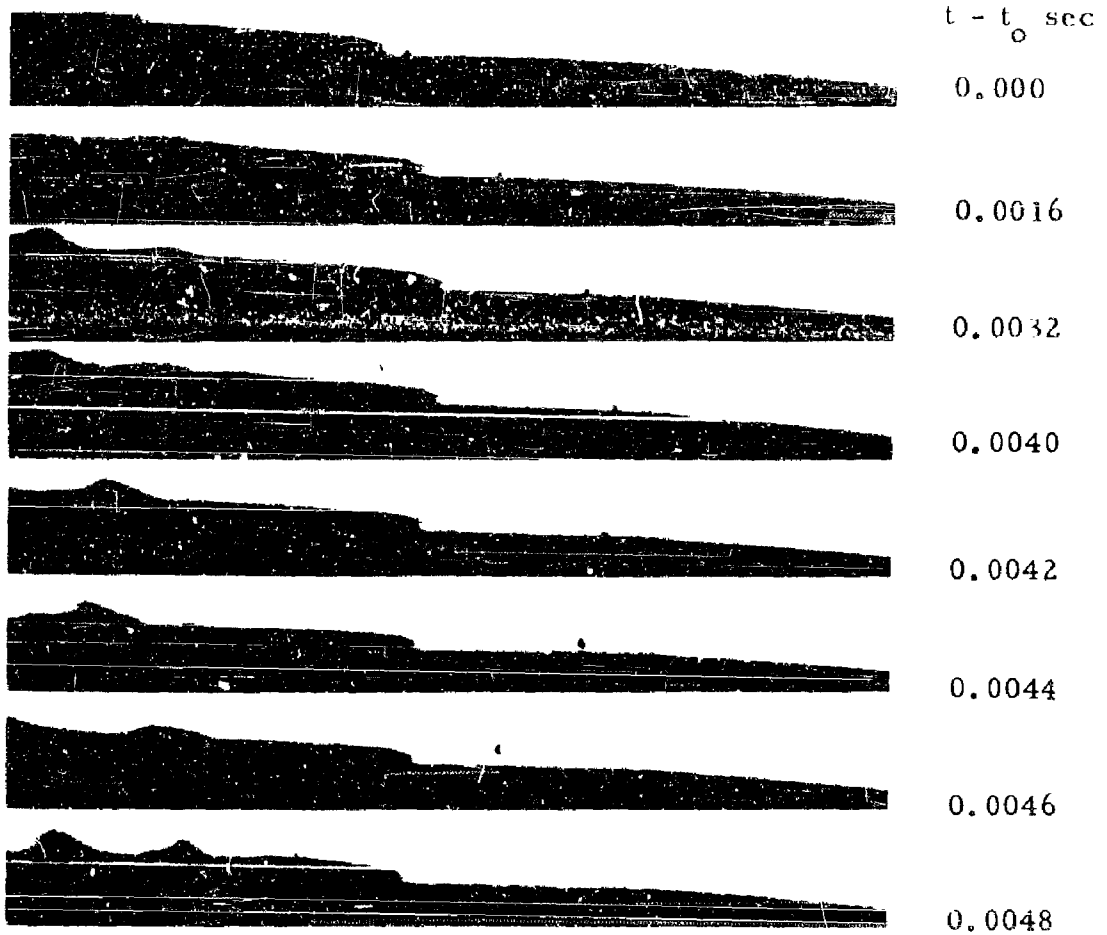


Fig. 14 - Microscopic cavitation bubble in secondary upstream motion.

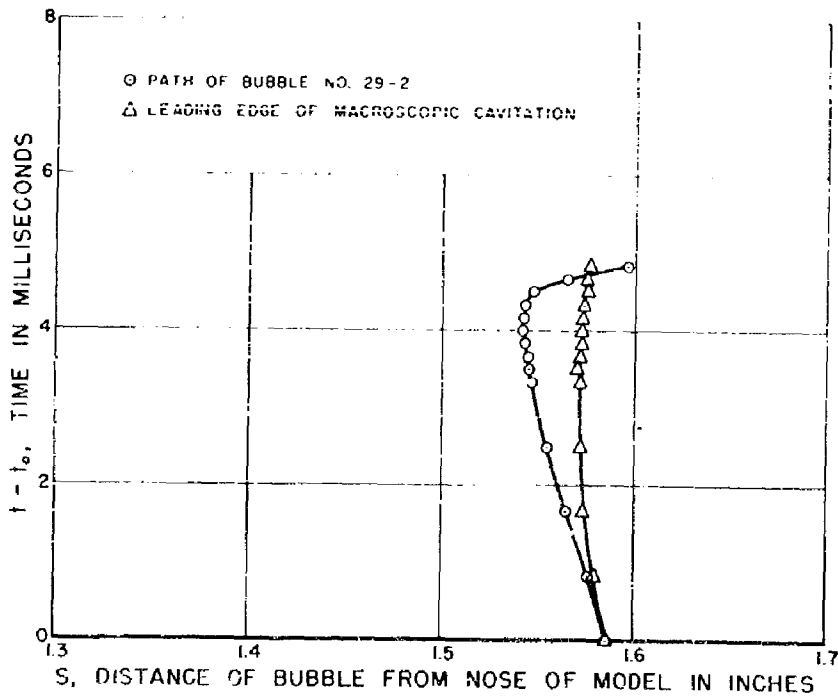


Fig. 15 - Position vs. time curve for bubble in secondary motion in the boundary layer for the bubble of Fig. 14.

taken at the first frame before the bubble separated from the macroscopic cavity. The curve of bubble progress and the position-time curve for the leading edge of the macroscopic cavity intersect when the small bubble was transported to a point directly above the leading edge of the macroscopic cavitation.

The Role of Air Diffusion in Cavitation Inception

The fact that cavitation bubble growth was observed in regions where the local pressure exceeds the vapor pressure of the water gave rise to the question of the possible role played by the diffusion of air into a bubble from the surrounding water. As noted above, a change in the air content of the tunnel water from 7.6 to 16.3 parts per million made no detectable difference in the sequence of events or the cavitation number at cavitation inception. Therefore a theoretical investigation was conducted to see if air diffusion could be an important factor in bubble growth despite the apparent insensitivity of cavitation inception to changes in air content. The dissolved air content of the water for the experiments of Fig. 10 was slightly supersaturated under a pressure of one atmosphere. Hence, at pressures between 40 and 80 millimeters of mercury the dissolved air concentration was between 10 and 20 times its saturation value at those pressures. In view of these very high supersaturations one might suppose that diffusion could easily account for the observed bubble growth. It appeared from the photographs that the size of the bubbles when they first become visible is roughly between one-third and one-fifth of their final size at breakaway. Calculations were made for such bubble growths under these conditions of supersaturation by the method of Epstein and Plesset⁶. However their method is only valid for the case when the liquid is stationary with respect to the bubble aside from motions due to bubble growth. It is therefore not surprising to find from such calculations that a growth time of the order of one second would be needed for the bubbles to attain a 0.002-in. diameter. Comparison of estimated bubble wall velocities with the liquid velocities in the boundary layer showed that the streaming flow around the top of the bubbles is much greater than any radial liquid velocity which could be due to bubble growth. Hence we must consider the effect of these streaming or liquid transport velocities upon the rate of air diffusion into a typical bubble. Because the streaming velocities over the tops of bubbles in the boundary layer are fairly high, no theoretical or experimental work could be found in the

literature from which we could obtain order of magnitude estimates for the effect of velocity on the diffusion rate. The results obtained from the Epstein-Plesset calculations indicated that appreciable air diffusion can occur only through those portions of the bubble wall where the liquid transport velocities are large. Accordingly, approximate calculations were made for air diffusion from a steady rectilinear flow of supersaturated water into a limited planar area which was parallel to the flow, and which represented the surface of a bubble. The calculations were made by two approximate methods.* Both of these calculations indicated that the observed bubble growth could be due to air diffusion. However, the experimental data were not sufficiently detailed and the diffusion calculations were not accurate enough to justify a definite conclusion, but there is enough experimental evidence at this time to make certain tentative conclusions about the role of air diffusion in the inception process.

As shown in a subsequent part of this report, the upstream pressure influence of a clear macroscopic cavity could suppress the growth of the small microscopic bubbles because the first appearance of the clear cavities attached to the body raises the pressure on the body upstream from the macroscopic cavitation zone. This would mean that the pressure on the body would be too high for the occurrence of dynamic bubble growth.

On the other hand, it has been shown that air diffusion may play an important part in the formation of the microscopic bubbles. Therefore one must consider the changes in the diffusion process which the appearance of the clear macroscopic cavitation could cause and the result of such changes upon the growth of the microscopic bubbles by air diffusion.

Suppose for the moment that the microscopic bubbles grow only by air diffusion. One must now decide how the first appearance of the clear macroscopic cavitation can affect this growth. Of course the relatively large clear cavity is sustained in part by a high rate of air diffusion which could conceivably lower the dissolved air concentration in the upstream region of microscopic cavitation. However, it turns out that the upstream influence of the macroscopic cavitation upon the dissolved air concentration is exponentially reduced. This severe reduction is caused by the liquid flow velocity in such a way that

*The author wish to acknowledge the assistance of Dr. Y. T. Wu with the diffusion calculations.

the change in air concentration decreases exponentially with the product of the velocity and the upstream distance from the macroscopic cavitation. Even though the microscopic bubbles are not too far upstream from the macroscopic zone, where the diffusion rate is probably very high, the appearance of clear macroscopic cavities can have little effect upon the dissolved air concentration in the region of microscopic cavitation.

The appearance of clear macroscopic cavitation can influence the degree of supersaturation of air in the water in a second way by the increase of pressure on the model which accompanies this change in the flow state. However, this pressure change is too small to alter radically the importance of air diffusion because the initial supersaturation is extremely high.

From these arguments it is evident that if the microscopic cavitation originates only from air diffusion, the microscopic bubbles should be little influenced by the onset of the clear macroscopic cavitation. This is contrary to observation. Instead it seems more likely that at inception the microscopic cavitation originates in regions of the boundary layer where the static pressure is less than the liquid vapor pressure; that is, initially the cavitation nuclei grow only by dynamic means. After these growing bubbles have been transported to the higher pressure zone where our observations were made, the process of air diffusion produces additional growth. Then when the cavitation number is lowered to the point where the macroscopic bubble becomes a clear cavity attached to the body, the microscopic cavitation disappears, not because air diffusion is suppressed, but because the pressure increase accompanying the formation of the clear macroscopic cavitation prevents the initial phase of dynamic bubble growth.

This view of the importance of air diffusion in the cavitation process throws some light on past observations which indicated that the dissolved air content of the tunnel water had no consistent effect on the incipient cavitation number of the scaling tests^{1, 2}. These tests were carried out over a range of air contents which was larger than that which one would expect to encounter in normal practice. Therefore it appears that normal variations in the dissolved air concentration will have no important effect on the incipient cavitation number for practical purposes. The experimental results from the tunnel seem reasonable if it is recognized that in the lowest pressure regions of the model the water was supersaturated by a factor of about twenty for the highest

dissolved air concentrations, and ten times supersaturated for the lowest concentrations. Even this lower supersaturation is so large that the diffusion process is relatively little affected by this twofold change. One can see that if water tunnel experiments are to show the effect of air concentration on cavitation inception, a practical way to drive almost all of the air from the tunnel water must be found.

The Need for Further Pressure Measurements

The growth of small bubbles in the boundary layer in the region upstream of the first visible macroscopic cavitation and the motions of some bubbles from the downstream macroscopic cavitation zone back into the upstream region have been observed. These observations point to the existence of pressures on the body which are less than the liquid vapor pressure. The existence of such tensions, or pressures less than the vapor pressure, in the liquid must occur if there is to be a motive force for bubble growth. Further, the fact that some bubbles have been observed to move in the upstream direction indicates that buoyant forces are acting upon these bubbles which can arise only if the pressure upstream of the macroscopic cavitation is lower than that in the region of the macroscopic cavitation. Thus if we suppose the zone of macroscopic cavitation to be at the vapor pressure, it follows that the liquid in the upstream region where there is bubble growth must experience a tension. However, no direct measurements of such pressures existed which could verify these inferences. Accordingly, it was decided to supplement the photographic study with additional pressure measurements.

The Shortcomings of Conventional Pressure Measurements

Previous investigators^{7, 8, 9} have reported that their measurements indicate that ordinary flowing water will not withstand a tension. However, their results depend upon the method of measurement in which conventional pressure taps were connected by water-filled lines to a suitable manometer. Such methods are not adequate for pressure measurements at cavitation inception.

In Goldstein¹⁰ the circumstances responsible for the usefulness of

common piezometer taps are described. The feature of most interest here is that steady flow over the tap induces a small vortex in the entrance of the tap. Under noncavitating conditions this eddy in the hole allows the outer flow over the body to remain undisturbed and the pressure in the manometer line corresponds to that of the flow next to the body. However, when the static pressure in a water tunnel working section is lowered, cavitation commences at those pressure taps situated in the region of lowest pressure on the model. Cavitation initiated from such taps invariably commences at a higher value of the free stream static pressure or cavitation number than would be the case for cavitation on the same body with no taps.

Past experience has shown that as the working section pressure was lowered, the first signs of cavitation appeared at the center of the vortex core inside the tap. When the pressure was lowered further, the cavitation spread from the vortex center until a small cavity attached itself to the piezometer hole and streamed back over the model surface. When this stage was reached the small attached cavity was sustained by evaporation from the cavity walls and the pressure in the manometer line must have equaled the liquid vapor pressure. Under these conditions the impure water in the manometer lines boils so that frequent manometer bleeding is required. Thus it is not surprising that the consistent data obtained by other investigators under these conditions have shown the lowest pressure coefficient on the body to be very near or equal to the negative of the measured cavitation number. Although previous results are probably reliable for large vapor cavities, evidently the conventional methods of measurement were not capable of providing correct values for the minimum pressure on the body under conditions of incipient cavitation.

Since the usual method of measurement cannot provide direct indications of the pressures on a body which is experiencing incipient cavitation, a modification of the ordinary method was tried. The most obvious remedy seemed to lie in the direction by which the effects of the piezometer vortex could be eliminated. It appeared that two simple steps might deal with the problem. First, the diameter of the pressure tap could be reduced and second, a fluid, other than water, with a very low vapor pressure could be used between the manometer and piezometer tap. Preliminary experiments with Dow Corning DC-200 fluid of 10 centistokes kinematic viscosity and pressure taps as small as 0.006 in. in diameter proved unsuccessful. Although reductions in tap diameter reduced the free stream static pressure at which the taps cavitared,

it was not found possible to suppress this premature cavitation even when the silicone fluid was forced from the tap into the stream.

Membrane Method for Measuring Pressure

Because of difficulties described above we decided to avoid entirely the hydrodynamic problem associated with ordinary pressure taps by interposing a thin membrane between the tap and the flow over the body, so that air pressure inside the tap could be used to balance the pressure in the water. We were reluctant to take this step because it seemed that we were substituting several new problems for one old difficulty. Our subsequent experience convinced us that this was indeed true. These problems have not yet been entirely solved, but we have been able to obtain direct qualitative proof of the existence of tensions in the flowing liquid under conditions of incipient cavitation. We believe that these first simple experiments have provided us with enough technical data to allow a solution for the remaining problems.

The model selected for the membrane pressure measurements was the same two-inch diameter brass hemisphere which was used in the noncavitating pressure distribution tests described above. Further, the model was side mounted in the working section so that membrane pressure measurements could be compared with the photographic findings and the noncavitating pressure distributions.

For small deflections, the rate of change of deflection with respect to pressure at the center of a circular membrane is equal to the square of the membrane diameter divided by the membrane tension. Hence for maximum sensitivity the diaphragm should have the largest diameter consistent with the model size or the nature of the pressure distribution in the vicinity of the membrane. For these experiments the minimum pressure point on the body was of primary interest since it is only near this point that the liquid will experience a tension. From Fig. 1 we see that the minimum pressure occurs at an S/R of 1.4 or 80.2° from the nose when the meridional section of the model is at 90° with the horizontal, see Appendix, Section A (Fig. 24). For this region on the body a $1/16$ in. diaphragm diameter seemed appropriate. Hence a $1/16$ diameter tap was drilled at this point and provisions were made for an air line between the tap and a mercury manometer outside the tunnel. Thus, when the membrane is cemented around the tap, the pressure of the

air-mercury system must balance the pressure in the water flow over the model when the membrane is in the null position. The membrane air pressure was adjusted by changing the level of the mercury reservoir as shown in Fig. 16. The value of the membrane air pressure was found by subtracting the difference in mercury levels ΔH from the barometric pressure. The position of the membrane during the tests was observed with a cathatometer telescope. A photograph of the complete test setup is shown in Fig. 17.

The detailed procedure developed for gluing membranes to the model can be found in Appendix, Section B. Figure 18 shows a photograph of a successful membrane on the model. The diaphragm is shown facing the camera. The model has been grooved about two diameters behind the tip of the nose so that the membrane could be bound to the model base. The distance of the groove from the nose was made as great as possible so the resulting disturbance to the flow over the nose would be negligible.

Pressure measurements made by the membrane technique in noncavitating flow were compared with similar measurements which are made by the conventional method. These tests showed that the membrane technique gave the pressure in the flow over the diaphragm with sufficient precision. Further, tests in air were made to determine the deflection of several membranes for various differential pressures across the diaphragm. These details of the membrane experiments are discussed in the Appendix, Section C.

Tension Measurements at Incipient Cavitation

The "Cenco Hyvac" vacuum pump which is indicated in the schematic diagram, Fig. 16, was needed only for the membrane pressure experiments in cavitating flow. The lowest absolute pressure obtainable with the pump employed in these tests was about 1-1/2 mm of mercury. However, for most runs a pressure of 3 or 4 mm of mercury was the lowest obtained. Even though these pressures are less than or equal to 1/6 of the water vapor pressure, the membrane was found to bulge between 6 and 7 thousandths of an inch under conditions of incipient cavitation, Fig. 19. As the free stream static pressure was lowered from the incipient value, the amount of macroscopic cavitation was seen to increase. When the macroscopic cavitation turned into small clear cavities attached to the model, and the growth of the small bubbles upstream in the boundary layer was thereby suppressed, the membrane bulge

was always seen to collapse suddenly into a form like that of Fig. 20.

From these observations only, and without detailed measurements, we may conclude that there are indeed tensions in the flowing liquid under conditions of incipient cavitation. However it is important to note that in both bulged and nulled positions the membrane disturbs the flow so that we can only draw general qualitative conclusions from such measurements. That is, we did not measure the liquid tensions which exist on a hemisphere in cavitating flow, but we did determine the pressures on similar but slightly perturbed shapes. The established precision of the measurements justifies such general conclusions.

For both of the membranes which were tested under noncavitating conditions, runs were made with various degrees of cavitation on the model. The first membrane was run at a free stream velocity of 40 ft/sec. For the second membrane, sets of cavitation data were taken at both 30 and 40 ft/sec.

When the membrane is bulged into a liquid flow the pressure over the membrane is not constant as was the case for the bulge calibration experiments (Fig. 25, Section C, of the Appendix). Thus the use of results from Fig. 25 to compensate the pressure measurements for membrane deflection is only approximately correct. Further, the bulge pressure which was used to correct the data was selected from the curve determined by the most sensitive membrane E at a deflection which was slightly less than half of the observed maximum bulge of 0.006 to 0.007 in. This procedure was followed to give a conservative estimate of the tension under conditions of incipient cavitation. Accordingly, a bulge calibration pressure of 5 cm of mercury was selected. Further, it was assumed that the membrane was nulled for those cases where the bulge had collapsed under conditions of more profuse cavitation because either the membrane was entirely obscured by the cavitation or we could not visually estimate the amount by which the membrane was sucked in.

The results of the cavitation experiments are shown in Fig. 21 in which the absolute pressure on the model is plotted against the cavitation number. Near the point of inception the pressure on the model appears to increase with the cavitation number, which is to be expected. For lower cavitation numbers the pressure on the model is essentially constant. We believe that these constant portions of the curves should be near or at the liquid vapor pressure, but the data could not show this for the reasons already stated. The portions of

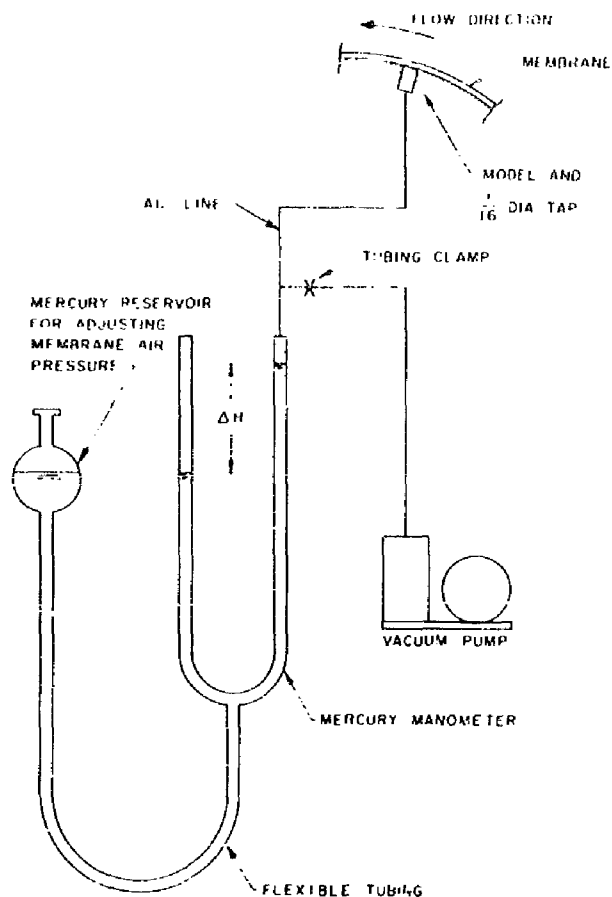


Fig. 16 - Schematic diagram of the apparatus used in the membrane method for measuring pressure on the model.

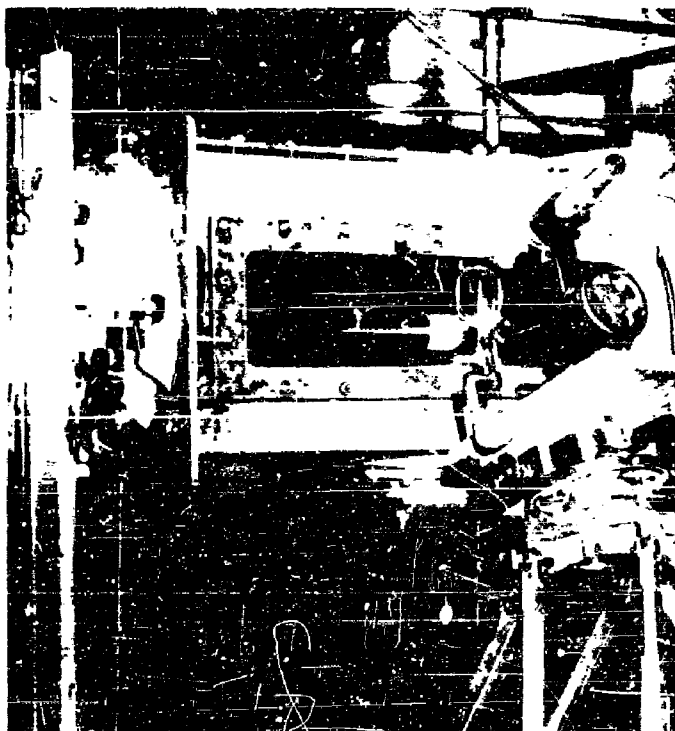


Fig. 17 - Setup for membrane pressure measurements.



Fig. 18 - Model with rubber membrane attached. Note pressure tap facing camera.



Fig. 19 - Incipient cavitation on model with rubber membrane. Note bulge at tap.

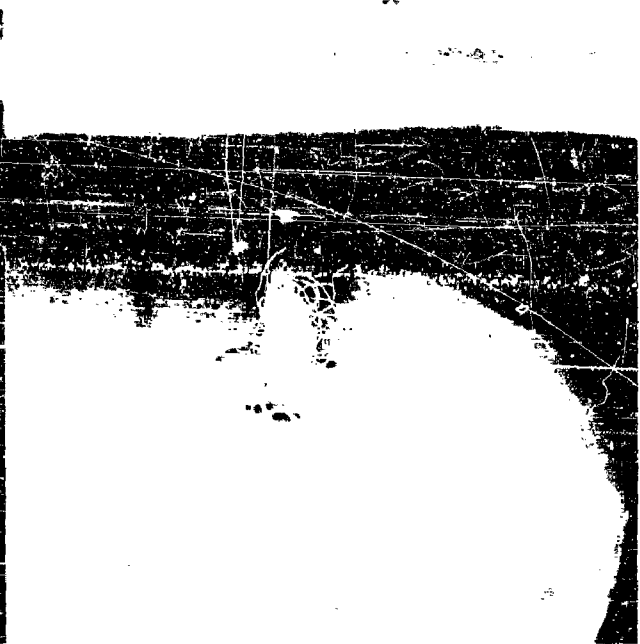


Fig. 20 - Attached cavity cavitation on model with membrane. Note diaphragm pushed into the tap.

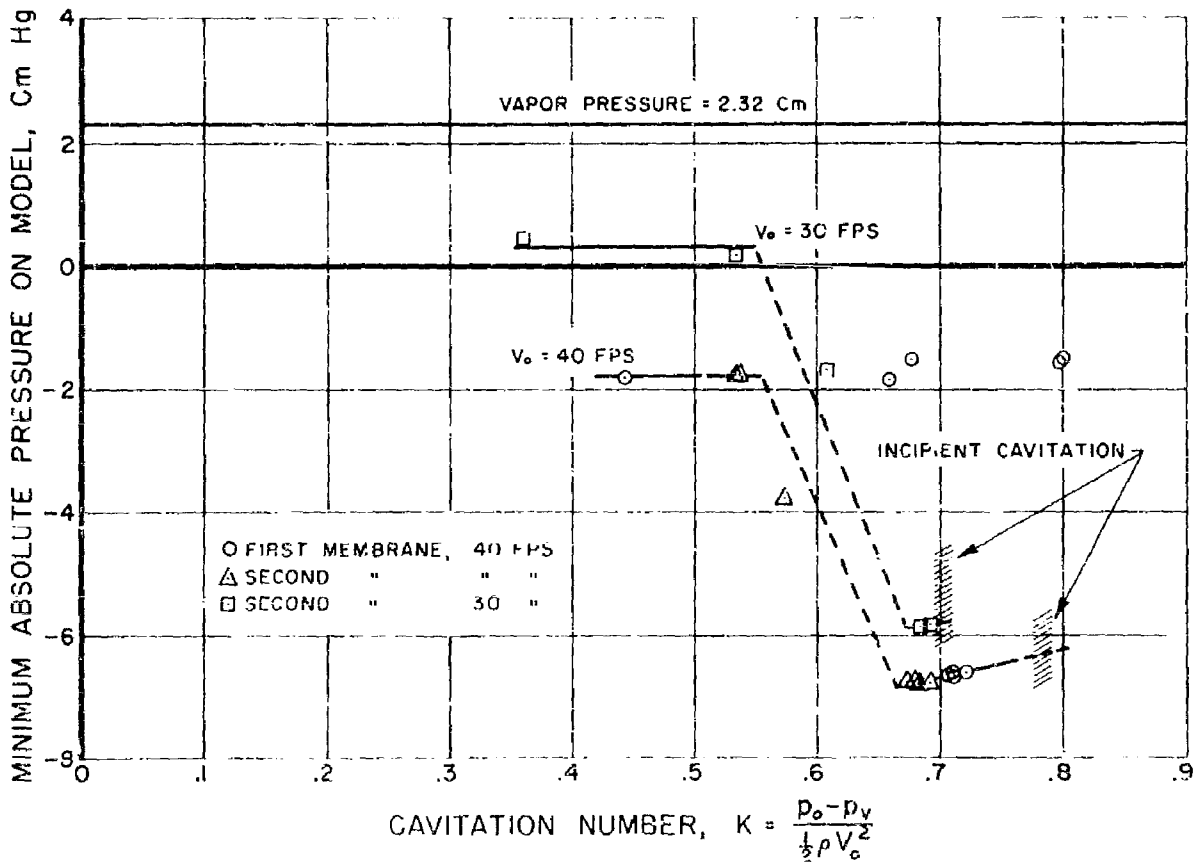


Fig. 21 - Minimum pressure measured on the model as a function of cavitation number.

the curves which corresponded to membrane collapse are shown by the dotted lines. These results provide direct experimental confirmation of the existence of liquid tensions in flowing water during incipient cavitation. In addition the reasons for the disappearance of the small bubbles in the boundary layer when the macroscopic cavitation first becomes a small clear cavity attached to the model have been experimentally verified.

Because of the limitations of the data mentioned above, no further conclusions can be drawn from the relative positions of the two curves of Fig. 21. More detailed conclusions must await the development of better instrumentation which is in progress. Even though it may be coincidental, it is interesting to note that from the steam tables¹¹ we find that the tensions given by Fig. 21 correspond to about 4°C superheat for boiling which is the same order of magnitude as those superheats found by Dergarabedian¹² in his boiling experiments. Also, if allowance is made for the differences in the value of the minimum pressure coefficients on a 1.5-caliber ogive and the present hemispheres, these measurements nearly check Plesset's¹³ assumption for the value of the water tension in his theoretical analysis of the experiments of Knapp and Hollander^{14*}.

* The bubbles studied by Knapp and Hollander were generated from small entrained air bubbles which moved over the model with the liquid outside of the boundary layer. One of the present authors observed in the course of cavitation research at the Ordnance Research Laboratory² that such large bubbles were distinct from and occurred at higher cavitation numbers than the cavitation which originates in the boundary layer. Further, it was found that the boundary layer cavitation occurred whether the cavitation resulting from entrained air was present or not so that the two effects appeared to be superposable. In fact, at the Ordnance Research Laboratory special measures were taken to drive the entrained air back into solution so that the cavitation which originates in the boundary layer could be easily observed. The present High Speed Water Tunnel does not allow the circulation of entrained air at normal air contents, with the result that the type of cavitation observed by Knapp and Hollander is seldom seen. Of course, such conditions of severe air entrainment could be encountered in practically important cases, such as in the wake of a ship. The purpose of this footnote is to call attention to the fact that the nature of cavitation inception is much different in the two cases.

Conclusions

The experiments thus far completed have provided the first results on the influence of the boundary layer on the inception of cavitation for smooth streamlined bodies. These experiments have shown that the neglect of the boundary layer in previous work was not justified. In addition, this study has given significant new information concerning the mechanics of cavitation inception.

The primary processes of cavitation inception on a smooth streamlined body may be summarized as follows. The inception of cavitation is characterized by two related processes. The first sign of incipient cavitation which is ordinarily visible to the unaided eye we call macroscopic cavitation. The fuzzy band of macroscopic cavitation is sustained by very small "microscopic" cavitation bubbles which grow in the boundary layer. The microscopic bubbles grow for a time at a fixed position on the body upstream from the macroscopic cavitation. Then when they attain a diameter roughly equal to the displacement thickness, they are lifted up slightly from the body, transported downstream and are distorted into irregular patches which sustain the macroscopic cavitation. When the free stream static pressure is lowered from the first inception point, the rate of microscopic bubble evolution increases and causes more profuse macroscopic cavitation until the macroscopic cavitation becomes a glassy cavity with its leading edge attached to the model. When this occurs, the microscopic cavitation is suppressed and macroscopic cavitation is sustained by evaporation and air diffusion through the cavity wall, as is the case for full cavity flow.

For the first time tensions have been observed and measured in the flow of ordinary water during incipient cavitation. These results show that the pressure distribution for noncavitating flow gives a good approximation to the actual pressures at cavitation inception as was assumed in Reference 3.

The tension measurements verify that when the macroscopic cavitation first becomes a clear attached cavity, the lowest pressure in the liquid increases so that bubble growth from dynamic causes cannot start. Hence the microscopic cavitation is suppressed by this pressure increase. However, it appears that the microscopic bubble growth observed so far is significantly influenced by air diffusion, but that these diffusion effects are important only in the later stages of growth. All of the experimental trends to date are

consistent with the view that the microscopic bubbles are originally vapor bubbles which grow because there is a pressure unbalance across the bubble wall. No observations of this early growth phase have yet been made.

The results which have been found thus far are not extensive enough to allow a complete analysis of cavitation inception to be made. In addition to more precise or more detailed data on the topics treated in this report, there are still many other problems which must be solved. For example, some of the future investigations must consider air diffusion, bubble dynamics, and the hydrodynamics of bubbles which are in the boundary layer. Research on these and other important aspects of the cavitation problem must be carried out if a complete theoretical explanation for the experimental scale effect observations is to be developed.

Appendix

A. Experimental Setup and Procedure

In order to obtain highly magnified photographs of microscopic cavitation on the model it was necessary to have the camera lens as close to the model nose as possible. For this reason the models used in these experiments were side mounted in the High Speed Water Tunnel working section. The same setup was used in the fully wetted pressure distribution runs, the dye studies, the tension tests and the photographic studies of cavitation.

The 2-in. diameter hemispherical head models were followed by a 4-in. long section of cylinder and a 10-1/2-in. long boom faired to a diameter of 1-1/3 in. The boom was fastened to a 2-in. span strut which was attached to the working section wall. This gave a clear length of 14-1/2 in. ahead of the support which should be sufficient to eliminate interference effects due to the strut.

Since most of the photographic work was done in silhouette the models were mounted with the top edge tangent to the horizontal axis or plane of the tunnel. This put the centerline of the models one inch below the tunnel centerline. At its nearest point the model was 1.02 in. from the working section wall, thus all parts of the model were outside the tunnel wall boundary layer. The line of symmetry of model and tunnel was 12 degrees below the horizontal axis of the tunnel. Figure 22 shows the relative position of all models in the tunnel.

The pressure distribution model had eleven pressure taps drilled alternately on opposite sides of the model in the same meridional plane. This method of placing the taps allowed the tap spacing to be as large as possible for the given number of taps. One-sixteenth in. outside diameter brass tubing and transparent plastic tubing was connected to the pressure taps and led outside the tunnel through the supporting boom and strut. Larger tubing led from the tunnel to the multi-tube manometer. All pressure data including velocity and p_0 were taken simultaneously by photographing the multi-tube manometer. The velocity was measured by connecting lines to piezometer rings at each end of the tunnel nozzle. The free stream static pressure p_0 was measured at a piezometer ring in the working section approximately 22 in. upstream from the model nose. The p_0 readings were corrected for the pressure drop along the working section to the position of the model nose.

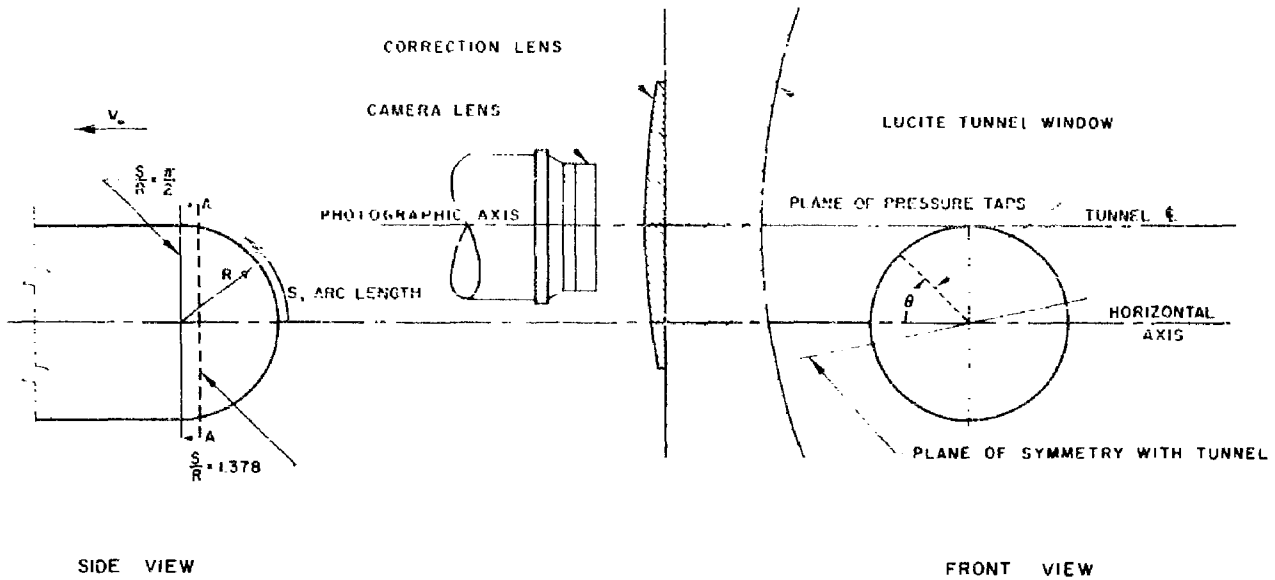


Fig. 22 - Sketch of setup with hemispherical model mounted near tunnel wall.

In order to get a complete survey of the pressure around the model and to study the effect of the proximity of the tunnel wall, pressure distribution runs were made at 5-degree intervals by rotating the model nose. Taking the horizontal plane as a zero, we defined the angle between the plane of the pressure taps and the horizontal plane as the polar angle θ , Fig. 22. Because of symmetry about the plane containing the axis of the tunnel and of the model, data were obtained only for values of the polar angle θ between -12° and 90° and between 168° and 270° . These data were reflected in the plane of symmetry to complete the entire pressure distribution. Duplicate runs were made for each θ setting and average values taken for the final results.

The pressure distribution model was also used to determine experimentally the zone of laminar-turbulent transition for noncavitating flow. A single pressure tap near the nose was connected to an accumulator filled with a saturated aqueous solution of potassium permanganate. Air pressure was used to inject a thin stream of dye into the boundary layer flow. Rapid diffusion of the dye filament indicated the transition point. Still photographs were taken to record these data.

In both the still and high-speed cavitation photographs the camera was positioned with an $f/4.5$ Micro Tessar shutterless lens approximately $1/4$ in.

from the outside surface of the lucite working section window. The inside surface of the working section lucite window is curved to fit the 14-in. diameter of the tunnel. The window has a minimum thickness of one inch with a flat outside surface. In order to reduce the distortion caused by the plano-concave cylindrical tunnel window, a 3-in. diameter glass plano-convex cylindrical correcting lens was taped to the outer flat surface of the working section window, Fig. 8. To provide precise, positive focusing, the high-speed camera was mounted on a slide, which in turn was mounted to a platform fastened to the tunnel working section.

B. A Method for Securing Rubber Membranes to the Model

The most difficult aspect of the tension experiments was that of attaching the membrane to the model so that it could not greatly disturb the flow. The membranes most successfully employed for this purpose were Trojan brand condoms because the rubber from which they are made is soft enough to be stretched over the model without tearing. It was necessary to cover the entire nose with the membrane and to get a strong bond over the nose so that the cavitation characteristics of the model would be unaffected. More than thirty membranes were cemented to the model before Mr. Wheeler, of the High Speed Water Tunnel staff, perfected a technique for bonding the membrane to the model strongly enough to meet the experimental requirements.

The following technique for cementing the membranes to the model was the most successful.

Three kinds of rubber cement were tried:

1. A and Aldite AN 101
Furane Plastics, Inc.
Glendale, California
2. Caram L 110
Made in Monrovia, California
3. DuPont Fairprine Cement Type No. 5128

We found the Fairprine to be best suited for the purpose. Further, we found that a better bond was obtained between rubber and brass than was obtained between rubber and steel.

The condom was cut so that a rectangular piece of rubber could be fitted on a four-inch embroidery hoop. The inside surfaces of the embroidery

hoop were covered with masking tape to avoid cutting the membrane. Then the Fairprine cement was diluted with carbon tetrachloride until it had the same consistency as SAE-20 or 10 oil. The membrane was painted on both sides with the diluted rubber cement. It has been found necessary to apply the Fairprine with care to small areas of the rubber until the whole membrane is covered because the solvent in the cement tends to dissolve the membrane and wrinkle it excessively. This procedure was made easier if the cement applied to the membrane was diluted to a thinner consistency than that specified above. The painted membrane was dried for twenty minutes. Evaporation of solvent from the cement solution caused its consistency to thicken. This thicker cement was applied to the model.

The model was next placed in a vise and the dilute cement poured evenly over it. The pressure tap was prevented from clogging by inserting a round tooth pick which was coated with grease or silicone fluid into the hole before the cement was applied. The cement was allowed to dry on the model for twenty minutes.

The membrane in the embroidery hoop was then pulled down even'y over the model and secured to the groove at its base by wrapping it with nylon thread. The thread was next covered with Duco cement.

The completed assembly was cured in an oven. The best bond was obtained when the model was baked at 175° for an hour and ten minutes. Because of the many variables involved in this procedure, we have not yet been able to attain uniform bond strengths. More work must be done before this technique can be perfected.

C. Proofing the Pressure Measuring Apparatus

The precision of pressure measurements under cavitating conditions may be determined by comparing the probable error with the liquid vapor pressure. Further, untried instrumentation should also be compared with known methods of measuring the desired quantity. These objectives were accomplished in this case by using the membrane technique to measure the minimum pressure on the model under noncavitating conditions. For these experiments it was very important to get enough data for a given flow condition because in addition to visual determination of the membrane null position, it was necessary to obtain three simultaneous manometer readings. These

factors and the usual pressure fluctuations in the tunnel allowed considerable latitude for experimental error. For these calibration experiments twenty sample points comprised each group of data. For each data group the free stream static pressure was varied systematically so that the membrane had to be nulled and the corresponding membrane air pressure readings recorded. This procedure allowed the error from these factors to be emphasized. Further, two membranes were fitted to the model so that some idea of variations in the data from differing membrane properties could be gained. All of these noncavitating pressure experiments were conducted with a free stream velocity of 40 fps so that the difference between the free stream static pressure and the minimum pressure on the model would be constant if there were no experimental errors. The first data for noncavitating flow was followed by cavitation tests and then the noncavitating pressure tests were repeated on the next day with the same membrane. The first set of twenty points is shown as a histogram in Fig. 23. The data for Δp , the difference between the free stream static pressure p_0 and the pressure on the diaphragm p , was classified into one millimeter intervals. For example, a point at 46.81 cm of mercury would fall into the class $46.8 < \Delta p \leq 46.9$. The mean for this first data was $\bar{\Delta p} = 46.77$ cm Hg. The confidence limits for this mean¹⁵ were calculated to be in the interval $46.29 < \bar{\Delta p} < 47.25$ when the probability that the mean will fall within these limits is 95%. On the basis of these results we may take for Δp the value 46.77 ± 0.48 cm of mercury. The relative error is $\pm 1.0\%$.

Similarly the data from the second set of twenty points from the first membrane gave the value $\Delta p = 46.49 \pm 0.64$ cm of mercury. The relative error was $\pm 1.4\%$. As can be seen, this second mean falls within the limits calculated from the first set of data.

When the second membrane was attached to the model, the set of twenty points in noncavitating flow gave $\Delta p = 47.89 \pm 0.13$ cm of mercury. The relative error was $\pm 0.3\%$. It will be seen that this value falls outside the limits found for the other membrane. However, the accuracy for this membrane was much better than the data for the first membrane. This improvement probably resulted from the better experimental technique which practice gave us. Thus we believe that this relative difference of 2.6% between the results from the two membranes may be caused by a difference in the properties of the membranes. The largest error in any of these experiments,

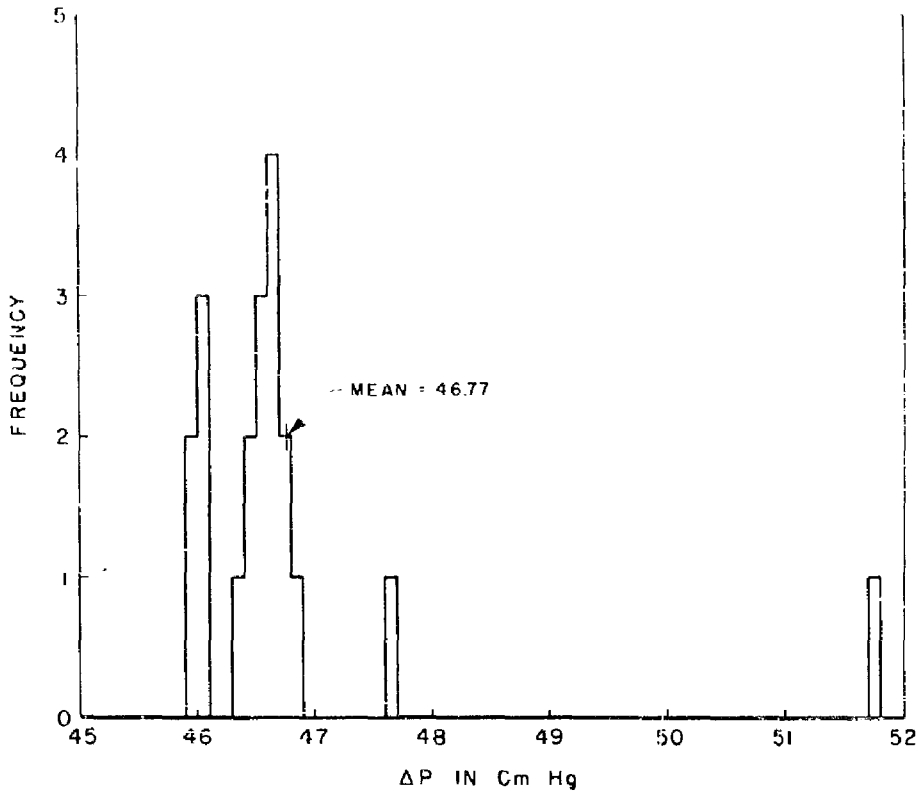


Fig. 23 - Histogram of data points obtained in membrane pressure tests,

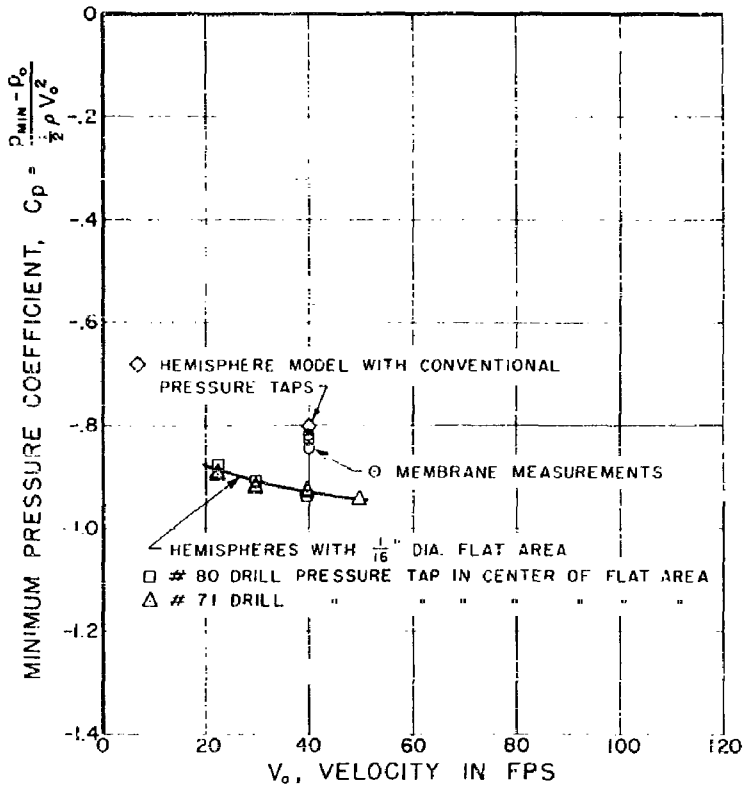


Fig. 24 - Minimum pressure coefficients on smooth model, model with membrane, and model with small flattened area around pressure tap.

± 6 mm of mercury, was about $1/4$ of the vapor pressure of water at 76.3° F. which was the average water temperature for these experiments. The least error, ± 1.3 mm of mercury, corresponded to about $1/18$ of the vapor pressure of water. Even the lowest precision achieved was adequate for the present purpose.

When these data were reduced to pressure coefficient form it was found that the value for the minimum C_p obtained in the usual way, Fig. 1, was higher than the values found with the membranes, Fig. 24. Of course, when readings are taken with a flat or null membrane, the shape of the nose is no longer hemispherical and a variation of the pressure on the flat region is to be expected. In order to determine the greatest possible effect when the nose has a small circular flat at the minimum pressure point, two hemispherical models with $1/16$ diameter pressure taps at the minimum pressure point were fabricated. These $1/16$ diameter holes were then fitted with cylindrical bushings so that the model curvature between the bushed flat area and the rest of the nose suffered a sharp discontinuity. In order that the effect of tap size could be estimated from these experiments, one model was provided with a tap of 0.0260 in. diameter (No. 71 drill) at the center of the flat while the other was drilled for a 0.0135 in. diameter (No. 80 drill) pressure tap. These models were side mounted in the tunnel with the tap polar angle θ at 90° as with the membrane tests and noncavitating pressure measurements were made at free stream velocities of 20, 30, 40 and 50 ft/sec. The relative differences because of pressure tap size were within 3% at all velocities.

All data for the minimum pressure coefficient under noncavitating conditions are compared in Fig. 24. The measurements made with the membrane are between the data from the hemisphere and the hemispheres with the $1/16$ in. diameter flat areas at the point of minimum pressure. At a free stream velocity of 40 ft/sec the presence of the flat spot causes the minimum pressure coefficient to decrease by 16% of its value on the undeformed hemisphere. Even though the membranes also caused the hemisphere to have a small flat area, the decrease in the minimum pressure from this cause was not as great as for the especially flattened models. Inspection of one of the membrane models with a Gaertner toolmaker's microscope showed that the membrane produced a continuous change in curvature between the spherical portion of the nose and the flat region of the nulled diaphragm. Thus, the relative positions of the various data are to be expected, and we believe that the pressure

in the liquid over the membrane is given within the limits of precision stated above.

It has been mentioned that one would expect the properties of one membrane to differ from those of others which have been stretched over a given model. However, except for the shape of the membrane near the tap, the null reading feature of the noncavitating pressure measurements should make the resulting data independent of other membrane properties. Hence it is reasonable to suppose that the definite small difference in the data from the two membranes was due only to a difference in shape.

Surprisingly enough, the tension in the stretched membranes is quite uniform, or perhaps we should say the ratio of membrane diameter squared to membrane tension shows small variations since this quantity determines the slope of the ΔH (pressure difference across the diaphragm) vs. membrane deflection line. This fact is shown by Fig. 25, for which five different membranes were cemented to the model and the maximum bulge for a given pressure differential was measured on the Gaertner toolmaker's microscope. These tests were performed in air and the same mercury manometer as was used for the tunnel tests was used for the differential pressure measurements. Each membrane was tested over its deflection range as many times as possible. All of the data for the five membranes fell along one line except membrane E and the first run of membrane A. The first run for membrane A did not give linear data and these data gave the steepest curve. After the first run the other data for membrane A fell in with the data for membranes B through D. We believe that the difference was caused by an excess of glue around the tap which loosened during the first deflection test. The data shows that membrane E was the most sensitive of the five. From this data the tension in membrane E was calculated to be 0.38 lbs/in.

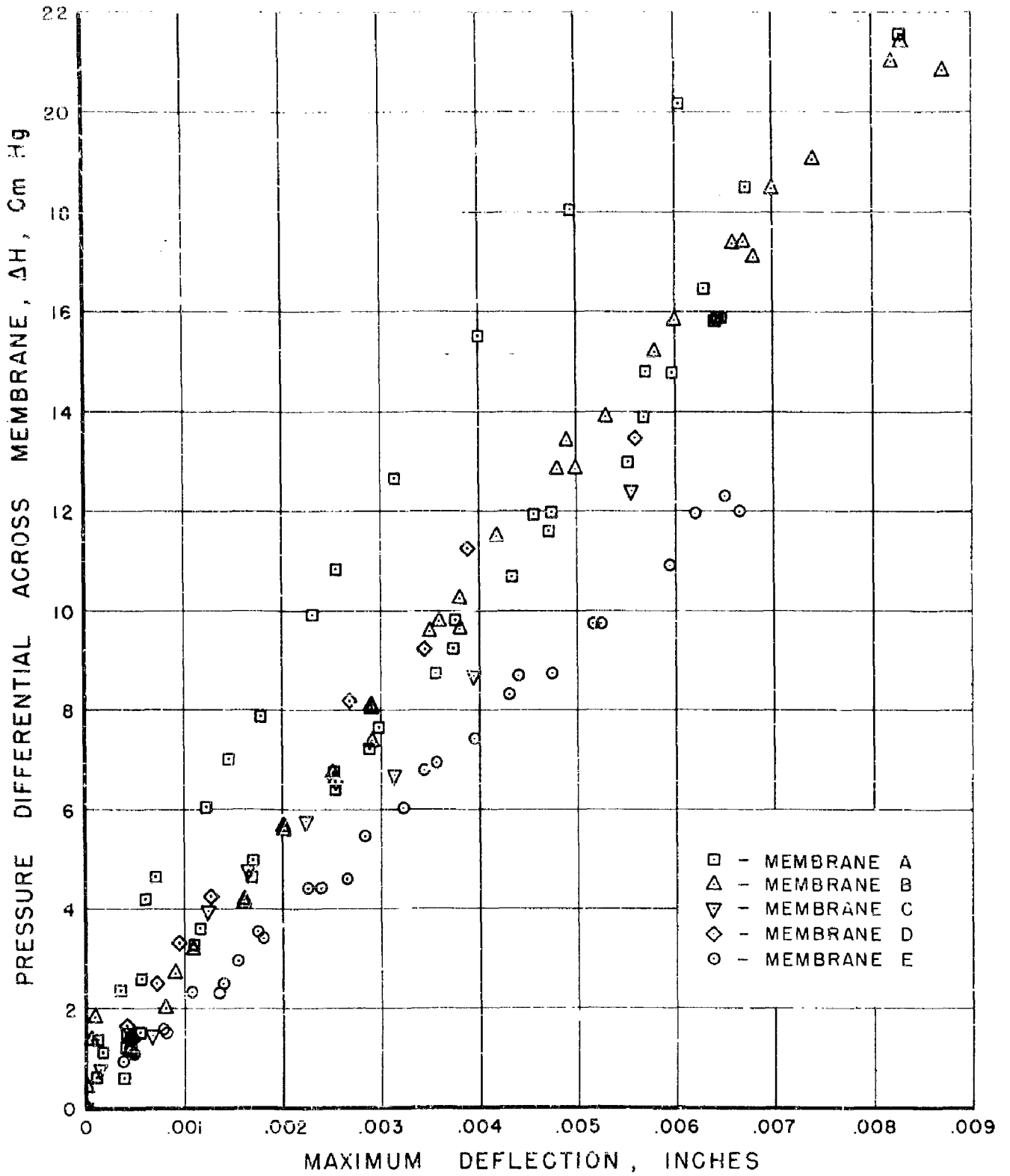


Fig. 25 - Deflection at the center vs the pressure across several membranes.

References

1. Kermeen, R. W., "Some Observations of Cavitation on Hemispherical Head Models", California Institute of Technology, Hydrodynamics Laboratory Report E-35, 1, June, 1952.
2. Farkin, B. R. and Holl, J. W., "Incipient-Cavitation Scaling Experiments for Hemispherical and 1.5-Caliber Ogive-Nosed Bodies", A Joint Study by The Hydrodynamics Laboratory, California Institute of Technology and The Ordnance Research Laboratory, The Pennsylvania State College, May, 1953.
3. Parkin, B. R., "Scale Effects in Cavitating Flow", California Institute of Technology, Hydrodynamics Laboratory Report No. 21-8, July, 1952.
4. Eisenberg, P., "An Asymptotic Solution for the Flow about an Ellipsoid near a Plane Wall", California Institute of Technology, Hydrodynamics Laboratory Report No. N-57, September, 1948. (Later published in J. Appl. Mech.)
5. Millikan, C. B., "The Boundary Layer and Skin Friction for a Figure of Revolution", Trans. Amer. Soc. Mech. Engineers, Applied Mech. Section 54 (1932).
6. Epstein, P. S., and Plesset, M. S., "On the Stability of Gas Bubbles in Liquid-Gas Solutions", J. Chem. Phys., Vol. 18, No. 11, pp. 1505-1509, November, 1950.
7. Ackeret, J., "Experimentelle Theoretische Untersuchungen über Kavitation", Techn. Mech. und Thermodyn., 1 (1930), 1-21 and 63-72.
8. Konstantinov, V. A., "Influence of Reynolds Number on the Separation (Cavitation) Flow" (1946). Translated by G. Weinblum, David W. Taylor Model Basin Translation 233, November, 1950.
9. Rouse, H. and McNown, J. S., "Cavitation and Pressure Distribution - Head Forms at Zero Angle of Yaw", Bulletin 32, State University of Iowa, Studies in Engineering.
10. Goldstein, S., "Modern Developments in Fluid Dynamics", Oxford University Press, 1938, p. 88.
11. Keenan, J. H. and Keys, F. G., "Thermodynamic Properties of Steam", John Wiley and Sons, Inc., 1936.
12. Dergarabedian, P., "The Rate of Growth of Vapor Bubbles in Superheated Water", California Institute of Technology, Hydrodynamics Laboratory Report No. 21-10, August, 1952.
13. Plesset, M. S., "The Dynamics of Cavitation Bubbles", J. Appl. Mech., Vol. 16, pp. 277-336, September, 1949.
14. Knapp, R. T. and Hollander, A., "Laboratory Investigations of the Mechanism of Cavitation", Trans. ASME, p. 419, July, 1948.
15. Hoel, P. G., "Introduction to Mathematical Statistics", John Wiley and Sons, New York, 1949, p. 144.

Armed Services Technical Information Agency

Because of our limited supply, you are requested to return this copy WHEN IT HAS SERVED YOUR PURPOSE so that it may be made available to other requesters. Your cooperation will be appreciated.

AD

36510

NOTICE: WHEN GOVERNMENT OR OTHER DRAWINGS, SPECIFICATIONS OR OTHER DATA ARE USED FOR ANY PURPOSE OTHER THAN IN CONNECTION WITH A DEFINITELY RELATED GOVERNMENT PROCUREMENT OPERATION, THE U. S. GOVERNMENT THEREBY INCURS NO RESPONSIBILITY, NOR ANY OBLIGATION WHATSOEVER; AND THE FACT THAT THE GOVERNMENT MAY HAVE FORMULATED, FURNISHED, OR IN ANY WAY SUPPLIED THE SAID DRAWINGS, SPECIFICATIONS, OR OTHER DATA IS NOT TO BE REGARDED BY IMPLICATION OR OTHERWISE AS IN ANY MANNER LICENSING THE HOLDER OR ANY OTHER PERSON OR CORPORATION, OR CONVEYING ANY RIGHTS OR PERMISSION TO MANUFACTURE, USE OR SELL ANY PATENTED INVENTION THAT MAY IN ANY WAY BE RELATED THERETO.

Reproduced by
DOCUMENT SERVICE CENTER
KNOTT BUILDING, DAYTON, 2, OHIO

UNCLASSIFIED